We are IntechOpen, the world's leading publisher of Open Access books Built by scientists, for scientists

4,800
Open access books available

122,000
International authors and editors

135M
Downloads

Our authors are among the

154
Countries delivered to

TOP 1%
most cited scientists

12.2%
Contributors from top 500 universities

CLARIVATE ANALYTICS BOOK CITATION INDEX INDEXED

WEB OF SCIENCE™

Selection of our books indexed in the Book Citation Index in Web of Science™ Core Collection (BKCI)

Interested in publishing with us?
Contact book.department@intechopen.com

Numbers displayed above are based on latest data collected.
For more information visit www.intechopen.com

Chapter 3

Multi-user MIMO in LTE and LTE-Advanced - Receiver Structure and Precoding Design

Rizwan Ghaffar, Raymond Knopp and Florian Kaltenberger

Additional information is available at the end of the chapter

http://dx.doi.org/10.5772/57134

1. Introduction

The spatial dimension surfacing from the usage of multiple antennas promises improved reliability, higher spectral efficiency [24], and the spatial separation of users [6]. This spatial dimension (MIMO) is particularly beneficial for precoding in the downlink of multi-user cellular systems (broadcast channel), where these spatial degrees of freedom at the transmitter can be used to transmit data to multiple users simultaneously. This is achieved by creating independent parallel channels to the users (canceling multi-user interference) and the users subsequently employ simplified single-user receiver structures. However, the transformation of cross-coupled channels into parallel non-interacting channels necessitates perfect channel state information at the transmitter (CSIT) whose acquisition in a practical system, in particular frequency division duplex (FDD) system, is far from realizable. The complexity associated with the feedback overhead coupled with the low rate feedback channels are the major impediments in CSIT acquisition. This leads to the precoding strategies based on the partial or quantized CSIT [15], which limit the gains of multi-user MIMO.

On the design of feedback, there is stark contrast between the theoretically established results and current standards. Theory has established that the amount of CSIT feedback in a downlink system needs to grow in proportion to the SNR [11] and otherwise the degrees of freedom are lost. However to avoid the burden of feedback and due to complexity constraints, the modern wireless systems have been restricted to fixed rate feedback schemes. With such premises, LTE and LTE-Advanced have focused on the structured precoder codebook based approach [17, 19] by using a small number of feedback bits. These LTE precoders are characterized by low-resolution and are further based on the principle of equal gain transmission (EGT). These precoders when employed for the multi-user MIMO mode of transmission are unable to cancel the multi-user interference thereby increasing the sub-optimality of conventional single-user detection. This fixed low-level quantization of LTE codebook, therefore, eclipses most of the benefits of multi-user MIMO and raises questions

about the feasibility of this mode of transmission [22, page 244]. This strong perception is based on the fact that users can not cooperate in multi-user scenario and further on the assumption that users employ simple single-user receivers.

In this chapter, we focus on a new paradigm of multi-user MIMO where users exploit the discrete structure of interference, instead of ignoring it or assuming it to be Gaussian and merging it in noise. We compare the two strategies of interference exploitation and interference cancellation in multi-user scenario. For the former, we look at low complexity multi-user detectors. Though multi-user detection has been extensively investigated in the literature for the uplink (multiple access channel), its related complexity has so far prohibited its employment in the downlink (broadcast channel). For the multiple access channel, several multi-user detection techniques exist in the literature starting from the optimal multi-user receivers [25] to their near-optimal reduced complexity counterparts (sphere decoders [3]). The complexity associated with these techniques led to the investigation of low-complexity solutions as sub-optimal linear multi-user receivers [20], iterative multi-user receivers [26, 28], and decision-feedback receivers [5, 12]. Since in practice, most wireless systems employ error control coding combined with the interleaving , recent work in this area has addressed multi-user detection for coded systems based on soft decisions [13, 23]. We focus in this chapter on a low-complexity interference-aware receiver structure which not only reduces one complex dimension of the system but is also characterized by exploiting the interference structure in the detection process. Considering this receiver structure, we investigate the effectiveness of the low-resolution LTE precoders for the multi-user MIMO mode and show that multi-user MIMO can bring significant gains in future wireless systems if the users resort to intelligent interference-aware detection as compared to the sub-optimal single-user detection.

In an effort of bridging the gap between the theoretical and practical gains of multi-user MIMO, this chapter investigates the structure of LTE codebook by analyzing the pairwise error probability (PEP) expressions. The analysis shows that LTE precoders suffer from the loss of diversity when being employed in multi-user MIMO transmission mode but no such loss is observed in single-user MIMO mode. Based on this analysis, a new codebook design is proposed and it is shown that with a nominal increase in the feedback, the performance of multi-user MIMO improves to within 1.5 dB from the lower bound (single-user MIMO). To verify the proposed codebook design, widely studied Gaussian random codebooks [11], [2] are considered for comparison. Note that though the overall discussion in this chapter has generally been on LTE and LTE-Advanced framework, the proposed feedback and precoding design can serve as a guideline for multi-user MIMO modes in any other modern wireless system which employs limited feedback schemes for CSIT acquisition.

2. LTE system model

2.1. LTE - A brief overview

In 3GPP LTE, a 2×2 configuration for MIMO is assumed as the baseline configuration, however configurations with four transmit or receive antennas are also foreseen and reflected in the specifications [17]. LTE restricts the transmission of maximum of two codewords in the downlink which can be mapped onto different layers where one codeword represents an output from the channel encoder. Number of layers available for the transmission is equal

http://dx.doi.org/10.5772/57134

to the rank of the channel matrix (maximum 4). In this chapter, we restrict ourselves to the baseline configuration with the eNodeB (LTE notation for the base station) equipped with 2 antennas while we consider single and dual antenna user equipments (UEs). Physical layer technology employed for the downlink in LTE is OFDMA combined with bit interleaved coded modulation (BICM) [4]. Several different transmission bandwidths are possible, ranging from 1.08 MHz to 19.8 MHz with the constraint of being a multiple of 180 kHz. Resource Blocks (RBs) are defined as groups of 12 consecutive resource elements (REs - LTE notation for the subcarriers) with a bandwidth of 180 kHz thereby leading to the constant RE spacing of 15 kHz. Approximately 4 RBs form a subband and the feedback is generally done on subband basis. Seven operation modes are specified in the downlink of LTE, however, we shall focus on the following four modes:

- **Transmission mode 2.** Fall-back transmit diversity. Transmission rank is 1, i.e. one codeword is transmitted by the eNodeB. Employs Alamouti space-time or space-frequency codes [1].
- **Transmission mode 4.** Closed-loop spatial multiplexing. Transmission rank is 2, i.e. two codewords are transmitted by the eNodeB to the UE in the single-user MIMO mode. UEs need to have minimum of two antennas.
- **Transmission mode 5.** Multi-user MIMO mode. Supports only rank-1 transmission, i.e. one codeword for each UE.
- **Transmission mode 6.** Closed-loop precoding for rank-1 transmission, i.e. one codeword for the UE in the single-user MIMO mode.

In the case of transmit diversity and closed-loop precoding, one codeword (data stream) is transmitted to each UE using Alamouti code in the former case and LTE precoders in the latter case. Time-frequency resources are orthogonal to the different UEs in these modes thereby avoiding interference in the system. However, in the multi-user MIMO mode, parallel codewords are transmitted simultaneously, one for each UE, sharing the same time-frequency resources. Note that LTE restricts the transmission of one codeword to each UE in the multi-user MIMO mode.

For closed-loop transmission modes (mode 4, 5 and 6), precoding mechanisms are employed at the transmit side with the objective of maximizing throughput. The precoding is selected and applied by the eNodeB to the data transmission to a target UE based on the channel feedback received from that UE. This feedback includes a precoding matrix indicator (PMI), a channel rank indicator (RI) and a channel quality indicator (CQI). PMI is an index in the codebook for the preferred precoder to be used by the eNodeB. The granularity for the computation and signaling of the precoding index can range from a couple of RBs to the full bandwidth. For transmission mode 5, the eNodeB selects the precoding matrix to induce high orthogonality between the codewords so that the interference between UEs is minimized. In transmission modes 4 and 6, the eNodeB selects the precoding vector/matrix such that codewords are transmitted to the corresponding UEs with maximum throughput.

In order to avoid excessive downlink signaling, transmission mode for each UE is configured semi-statically via higher layer signaling, i.e. it is not allowed for a UE to be scheduled in one subframe in the multi-user MIMO mode and in the next subframe in the single-user MIMO mode. For transmission modes 4, 5 and 6, low-resolution precoders are employed which are based on the principle of EGT. For the case of eNodeB with two antennas, LTE

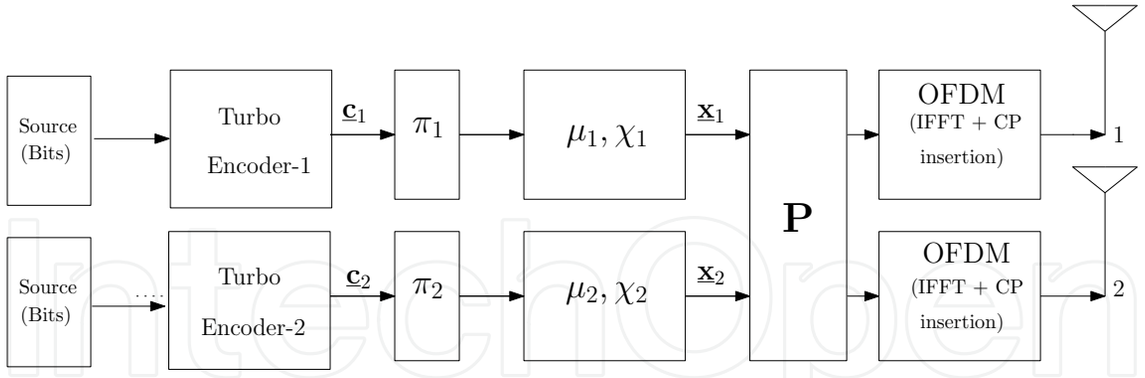

Figure 1. eNodeB in multi-user MIMO mode. π_1 denotes the random interleaver, μ_1 the labeling map and χ_1 the signal set for the codeword of UE-1. **P** indicates the precoding matrix.

proposes the use of following four precoders for transmission mode 5 and 6:

$$\mathbf{p} = \left\{ \frac{1}{\sqrt{4}} \begin{bmatrix} 1 \\ 1 \end{bmatrix}, \frac{1}{\sqrt{4}} \begin{bmatrix} 1 \\ -1 \end{bmatrix}, \frac{1}{\sqrt{4}} \begin{bmatrix} 1 \\ j \end{bmatrix}, \frac{1}{\sqrt{4}} \begin{bmatrix} 1 \\ -j \end{bmatrix} \right\} \tag{1}$$

The number of precoders increases to sixteen in the case of four transmit antennas however in this chapter we restrict to the case of two transmit antennas. For transmission mode 4, LTE proposes the use of following two precoder matrices on subband basis.

$$\mathbf{P} = \left\{ \frac{1}{\sqrt{4}} \begin{bmatrix} 1 & 1 \\ 1 & -1 \end{bmatrix}, \frac{1}{\sqrt{4}} \begin{bmatrix} 1 & 1 \\ j & -j \end{bmatrix} \right\} \tag{2}$$

Note that there is a possibility of swapping the columns in **P** but the swap must occur over the entire band.

2.2. System model

We first consider the system model for transmission mode 5, i.e. the multi-user MIMO mode in which the eNodeB transmits one codeword each to two single-antenna UEs using the same time-frequency resources. Transmitter block diagram is shown in Fig. 1. During the transmission for UE-1, the code sequence $\underline{\mathbf{c}}_1$ is interleaved by π_1 and is then mapped onto the signal sequence $\underline{\mathbf{x}}_1$. x_1 is the symbol of $\underline{\mathbf{x}}_1$ over a signal set $\chi_1 \subseteq \mathcal{C}$ with a Gray labeling map where $|\chi_1| = M_1$ and x_2 is the symbol of $\underline{\mathbf{x}}_2$ over signal set χ_2 where $|\chi_2| = M_2$. The bit interleaver for UE-1 can be modeled as $\pi_1 : k^{'} \rightarrow (k, i)$ where $k^{'}$ denotes the original ordering of the coded bits $c_{k^{'}}$, k denotes the RE of the symbol $x_{1,k}$ and i indicates the position of the bit $c_{k^{'}}$ in the symbol $x_{1,k}$. Note that each RE corresponds to a symbol from a constellation map χ_1 for UE-1 and χ_2 for UE-2. Selection of the normal or extended cyclic prefix (CP) for each OFDM symbol converts the downlink frequency-selective channel into parallel flat fading

http://dx.doi.org/10.5772/57134

channels. Cascading IFFT at the eNodeB and FFT at the UE with the cyclic prefix extension, the transmission at the k-th RE for UE-1 in transmission mode 5 can be expressed as

$$y_{1,k} = \mathbf{h}_{1,k}^{\dagger}\mathbf{p}_{1,k}x_{1,k} + \mathbf{h}_{1,k}^{\dagger}\mathbf{p}_{2,k}x_{2,k} + z_{1,k} \tag{3}$$

where $y_{1,k}$ is the received symbol at UE-1 and $z_{1,k}$ is zero mean circularly symmetric complex white Gaussian noise of variance N_0. $x_{1,k}$ is the complex symbol for UE-1 with the variance σ_1^2 and $x_{2,k}$ is the complex symbol for UE-2 with the variance σ_2^2. $\mathbf{h}_{n,k}^{\dagger} \in \mathbb{C}^{1\times 2}$ symbolizes the spatially uncorrelated flat Rayleigh fading MISO channel from eNodeB to the n-th UE ($n = 1, 2$) at the k-th RE. Its elements can therefore be modeled as independent and identically distributed (iid) zero mean circularly symmetric complex Gaussian random variables with a variance of 0.5 per dimension. Note that $\mathbb{C}^{1\times 2}$ denotes a 2-dimensional complex space. $\mathbf{p}_{n,k}$ denotes the precoding vector for the n-th UE at the k-th RE and is given by (1). For the dual antenna UEs, the system equation for transmission mode 5 is modified as

$$\mathbf{y}_{1,k} = \mathbf{H}_{1,k}\left[\mathbf{p}_{1,k}x_{1,k} + \mathbf{p}_{2,k}x_{2,k}\right] + \mathbf{z}_{1,k} \tag{4}$$

where $\mathbf{y}_{1,k}, \mathbf{z}_{1,k} \in \mathbb{C}^{2\times 1}$ are the vectors of the received symbols and circularly symmetric complex white Gaussian noise of double-sided power spectral density $N_0/2$ at the 2 receive antennas of UE-1 respectively. $\mathbf{H}_{1,k} \in \mathbb{C}^{2\times 2}$ is the channel matrix from eNodeB to UE-1.

In transmission mode 6, only one UE will be served in one time-frequency resource. Therefore the system equation for single-antenna UEs at the k-th RE is given as

$$y_k = \mathbf{h}_k^{\dagger}\mathbf{p}_k x_k + z_k \tag{5}$$

where $\mathbf{p}_k$ is given by (1). For the dual antenna UEs, the system equation for mode 6 is modified as

$$\mathbf{y}_k = \mathbf{H}_k\mathbf{p}_k x_k + \mathbf{z}_k \tag{6}$$

3. Multi-user MIMO mode

We now look at the effectiveness of the low-resolution LTE precoders for the multi-user MIMO mode. We first consider a geometric scheduling strategy [8] based on the selection of UEs with orthogonal precoders.

3.1. Scheduling strategy

As the processing at the UE is performed on a RE basis for each received OFDM symbol, the dependency on RE index can be ignored for notational convenience. The system equation for the case of single-antenna UEs for the multi-user mode is

$$y_1 = \mathbf{h}_1^{\dagger}\mathbf{p}_1 x_1 + \mathbf{h}_1^{\dagger}\mathbf{p}_2 x_2 + z_1 \tag{7}$$

The scheduling strategy is based on the principle of maximizing the desired signal strength while minimizing the interference strength. As the decision to schedule a UE in the single-user MIMO, multi-user MIMO or transmit diversity mode will be made by the eNodeB, each UE would feedback the precoder which maximizes its received signal strength. So this selected precoder by the UE would be the one closest to its matched filter (MF) precoder in terms of the Euclidean distance.

For the multi-user MIMO mode, the eNodeB needs to ensure good channel separation between the co-scheduled UEs. Therefore the eNodeB schedules two UEs on the same RBs which have requested opposite (orthogonal) precoders, i.e. the eNodeB selects as the second UE to be served in each group of allocatable RBs, one of the UEs whose requested precoder $\mathbf{p}_2$ is 180° out of phase from the precoder $\mathbf{p}_1$ of the first UE to be served on the same RBs. So if UE-1 has requested $\mathbf{p}_1 = \frac{1}{\sqrt{4}}\begin{bmatrix}1\\ q\end{bmatrix}, \quad q \in \{\pm 1, \pm j\}$, then eNodeB selects the second UE which has requested $\mathbf{p}_2 = \frac{1}{\sqrt{4}}\begin{bmatrix}1\\ -q\end{bmatrix}$. This transmission strategy also remains valid also for the case of dual-antenna UEs where the UEs feedback the indices of the precoding vectors which maximize the strength of their desired signals, i.e. $\|\mathbf{Hp}\|^2$. For the multi-user MIMO mode, the eNodeB schedules two UEs on the same RE which have requested 180° out of phase precoders. The details of this geometric scheduling strategy can be found in [7].

Though this precoding and scheduling strategy would ensure minimization of the interference under the constraint of low-resolution LTE precoders, the residual interference would still be significant. Single-user detection i.e. Gaussian assumption of the residual interference and its subsequent absorption in noise would lead to significant degradation in the performance. On the other hand, this residual interference is actually discrete belonging to a finite alphabet and its structure can be exploited in the detection process. However intelligent detection based on its exploitation comes at the cost of enhanced complexity. Here we propose a low-complexity interference-aware receiver structure [9] which on one hand reduces one complex dimension of the system while on the other hand, it exploits the interference structure in the detection process.

3.2. Low-complexity interference-aware receiver

First we consider the case of single-antenna UEs. Soft decision of the bit $c_{k'}$ of x_1, also known as log-likelihood ratio (LLR), is given as

$$\mathsf{LLR}_1^i\left(c_{k'}|y_1, \mathbf{h}_1^\dagger, \mathbf{P}\right) = \log \frac{p\left(c_{k'} = 1|y_1, \mathbf{h}_1^\dagger, \mathbf{P}\right)}{p\left(c_{k'} = 0|y_1, \mathbf{h}_1^\dagger, \mathbf{P}\right)} \tag{8}$$

We introduce the notation $\Lambda_1^i\left(y_1, c_{k'}\right)$ for the bit metric which is developed on the lines similar to the equations (7) and (9) in [4], i.e.

http://dx.doi.org/10.5772/57134

$$\begin{aligned}\Lambda_1^i\left(y_1, c_{k'}\right) &= \log p\left(c_{k'}|y_1, \mathbf{h}_1^\dagger, \mathbf{P}\right)\\ &\approx \log p\left(y_1|c_{k'}, \mathbf{h}_1^\dagger, \mathbf{P}\right)\\ &= \log \sum_{x_1 \in \chi_{1,c_{k'}}^i} \sum_{x_2 \in \chi_2} p\left(y_1|x_1, x_2, \mathbf{h}_1^\dagger, \mathbf{P}\right)\\ &\approx \min_{x_1 \in \chi_{1,c_{k'}}^i, x_2 \in \chi_2} \frac{1}{N_0}\left|y_1 - \mathbf{h}_1^\dagger \mathbf{p}_1 x_1 - \mathbf{h}_1^\dagger \mathbf{p}_2 x_2\right|^2 \end{aligned} \quad (9)$$

where $\chi_{1,c_{k'}}^i$ denotes the subset of the signal set $x_1 \in \chi_1$ whose labels have the value $c_{k'} \in \{0,1\}$ in the position i. Here we have used the log-sum approximation, i.e. $\log \sum_j z_j = \max_j \log z_j$ and this bit metric is therefore termed as max log MAP bit metric. As LLR is the difference of two bit metrics and these will be decoded using a conventional soft-decision Viterbi algorithm, $\frac{1}{N_0}$ (a common scaling factor to all LLRs) can be ignored thereby leading to

$$\begin{aligned}\Lambda_1^i\left(y_1, c_{k'}\right) &\approx \min_{x_1 \in \chi_{1,c_{k'}}^i, x_2 \in \chi_2}\left|y_1 - \mathbf{h}_1^\dagger \mathbf{p}_1 x_1 - \mathbf{h}_1^\dagger \mathbf{p}_2 x_2\right|^2\\ &= \min_{x_1 \in \chi_{1,c_{k'}}^i, x_2 \in \chi_2}\left\{|y_1|^2 + \left|\mathbf{h}_1^\dagger \mathbf{p}_1 x_1\right|^2 + \left|\mathbf{h}_1^\dagger \mathbf{p}_2 x_2\right|^2 - 2\left(\mathbf{h}_1^\dagger \mathbf{p}_1 x_1 y_1^*\right)_R + 2\left(\rho_{12} x_1^* x_2\right)_R - 2\left(\mathbf{h}_1^\dagger \mathbf{p}_2 x_2 y_1^*\right)_R\right\}\end{aligned} \quad (10)$$

where $\rho_{12} = \left(\mathbf{h}_1^\dagger \mathbf{p}_1\right)^* \mathbf{h}_1^\dagger \mathbf{p}_2$ indicates the cross correlation between the two effective channels. Here we have used the relation $|a-b|^2 = |a|^2 + |b|^2 - 2\left(a^* b\right)_R$ where the subscript $(.)_R$ indicates the real part. Note that the complexity of the calculation of bit metric (10) is $\mathcal{O}\left(|\chi_1|\,|\chi_2|\right)$.

In (10), we now introduce two terms as the outputs of MF, i.e. $\overline{y}_1 = \left(\mathbf{h}_1^\dagger \mathbf{p}_1\right)^* y_1$ and $\overline{y}_2 = \left(\mathbf{h}_1^\dagger \mathbf{p}_2\right)^* y_1$. Ignoring $|y_1|^2$ (independent of the minimization operation), the bit metric is written as

$$\Lambda_1^i\left(y_1, c_{k'}\right) \approx \min_{x_1 \in \chi_{1,c_{k'}}^i, x_2 \in \chi_2}\left\{\left|\mathbf{h}_1^\dagger \mathbf{p}_1 x_1\right|^2 + \left|\mathbf{h}_1^\dagger \mathbf{p}_2 x_2\right|^2 - 2\left(\overline{y}_1^* x_1\right)_R + 2\psi_A x_{2,R} + 2\psi_B x_{2,I}\right\} \quad (11)$$

where

$$\begin{aligned}\psi_A &= \rho_{12,R} x_{1,R} + \rho_{12,I} x_{1,I} - \overline{y}_{2,R}\\ \psi_B &= \rho_{12,R} x_{1,I} - \rho_{12,I} x_{1,R} - \overline{y}_{2,I}\end{aligned}$$

Note that the subscript $(.)_I$ indicates the imaginary part.

For x_1 and x_2 belonging to equal energy alphabets, $\left|\mathbf{h}_1^{\dagger}\mathbf{p}_1 x_1\right|^2$ and $\left|\mathbf{h}_1^{\dagger}\mathbf{p}_2 x_2\right|^2$ can be ignored as they are independent of the minimization operation. The values of $x_{2,R}$ and $x_{2,I}$ which minimize (11) need to be in the opposite directions of ψ_A and ψ_B respectively thereby avoiding search on the alphabets of x_2 and reducing one complex dimension in the detection, i.e.

$$\Lambda_1^i\left(y_1, c_{k'}\right) \approx \min_{x_1 \in \chi^i_{1,c_{k'}}} \left\{ -2\overline{y}_{1,R} x_{1,R} - 2\overline{y}_{1,I} x_{1,I} - 2\left|\psi_A\right| \left|x_{2,R}\right| - 2\left|\psi_B\right| \left|x_{2,I}\right| \right\} \tag{12}$$

As an example we consider the case of QPSK for which the values of $x_{2,R}$ and $x_{2,I}$ are $\left[\pm\frac{\sigma_2}{\sqrt{2}}\right]$, so the bit metric is written as

$$\Lambda_1^i\left(y_1, c_{k'}\right) \approx \min_{x_1 \in \chi^i_{1,c_{k'}}} \left\{ -2\overline{y}_{1,R} x_{1,R} - 2\overline{y}_{1,I} x_{1,I} - \sqrt{2}\sigma_2 \left|\psi_A\right| - \sqrt{2}\sigma_2 \left|\psi_B\right| \right\} \tag{13}$$

For x_1 and x_2 belonging to non-equal energy alphabets, the bit metric is same as (13) but $\left|\mathbf{h}_1^{\dagger}\mathbf{p}_1 x_1\right|^2$ and $\left|\mathbf{h}_1^{\dagger}\mathbf{p}_2 x_2\right|^2$ can no longer be ignored thereby leading to

$$\begin{aligned}\Lambda_1^i\left(y_1, c_{k'}\right) \approx \min_{x_1 \in \chi^i_{1,c_{k'}}} \Bigg\{ &\left|\mathbf{h}_1^{\dagger}\mathbf{p}_1\right|^2 |x_{1,R}|^2 + \left|\mathbf{h}_1^{\dagger}\mathbf{p}_1\right|^2 |x_{1,I}|^2 + \left|\mathbf{h}_1^{\dagger}\mathbf{p}_2\right|^2 |x_{2,R}|^2 + \left|\mathbf{h}_1^{\dagger}\mathbf{p}_2\right|^2 |x_{2,I}|^2 - \\ &2\overline{y}_{1,R} x_{1,R} - 2\overline{y}_{1,I} x_{1,I} - 2\left|\psi_A\right| \left|x_{2,R}\right| - 2\left|\psi_B\right| \left|x_{2,I}\right| \Bigg\}\end{aligned} \tag{14}$$

Note that the minimization is independent of χ_2 though x_2 appears in the bit metric. The reason of this independence is as follows. The decision regarding the signs of $x_{2,R}$ and $x_{2,I}$ in (14) will be taken in the same manner as for the case of equal energy alphabets. For finding their magnitudes that minimize the bit metric (14), it is the minimization problem of a quadratic function, i.e. differentiating (14) w.r.t $|x_{2,R}|$ and $|x_{2,I}|$ to find the global minimas which are given as

$$|x_{2,R}| \rightarrow \frac{|\psi_A|}{\left|\mathbf{h}_1^{\dagger}\mathbf{p}_2\right|^2}, \qquad |x_{2,I}| \rightarrow \frac{|\psi_B|}{\left|\mathbf{h}_1^{\dagger}\mathbf{p}_2\right|^2} \tag{15}$$

where $\rightarrow$ indicates the discretization process in which amongst the finite available points of $x_{2,R}$ and $x_{2,I}$, the point closest to the calculated continuous value is selected. So if x_2 belongs to QAM256, then instead of searching 256 constellation points for the minimization of (14),

http://dx.doi.org/10.5772/57134

the metric (15) reduces it to merely two operations thereby trimming down one complex dimension in the detection, i.e. the detection complexity is independent of $|\chi_2|$ and reduces to $\mathcal{O}(|\chi_1|)$.

As a particular example of the discretization of continuous values in (15), we consider the case of x_2 belonging to QAM16 . The values of $x_{2,R}$ and $x_{2,I}$ for the case of QAM16 are $\left[\pm\frac{\sigma_2}{\sqrt{10}}, \pm\frac{3\sigma_2}{\sqrt{10}}\right]$ so their magnitudes in (14) are given as

$$|x_{2,R}| = \sigma_2 \frac{1}{\sqrt{10}} \left(2 + (-1)^{I\left(|\psi_A| < \sigma_2 \frac{2\left|\mathbf{h}_1^\dagger \mathbf{p}_2\right|^2}{\sqrt{10}}\right)}\right)$$
$$|x_{2,I}| = \sigma_2 \frac{1}{\sqrt{10}} \left(2 + (-1)^{I\left(|\psi_B| < \sigma_2 \frac{2\left|\mathbf{h}_1^\dagger \mathbf{p}_2\right|^2}{\sqrt{10}}\right)}\right) \tag{16}$$

and $I(.)$ is the indicator function defined as

$$I(a < b) = \begin{cases} 1 \text{ if } a < b \\ 0 \text{ otherwise} \end{cases}$$

Now we look at the receiver structure for the case of dual-antenna UEs. The system equation for UE-1 (ignoring the RE index) is

$$\mathbf{y}_1 = \mathbf{H}_1 \left[\mathbf{p}_1 x_1 + \mathbf{p}_2 x_2\right] + \mathbf{z}_1 \tag{17}$$

The receiver structure would remain same with $\mathbf{h}_1^\dagger$ being replaced by $\mathbf{H}_1$, i.e. the channel from eNodeB to the two antennas of UE-1. Subsequently $\overline{y}_1 = (\mathbf{H}_1\mathbf{p}_1)^\dagger \mathbf{y}_1$ and $\overline{y}_2 = (\mathbf{H}_1\mathbf{p}_2)^\dagger \mathbf{y}_1$ are the MF outputs while $\rho_{12} = (\mathbf{H}_1\mathbf{p}_1)^\dagger \mathbf{H}_1\mathbf{p}_2$ is the cross-correlation between two effective channels.

For comparison purposes, we also consider the case of single-user receiver, for which the bit metric is given as

$$\Lambda_1^i(y_1, c_{k'}) \approx \min_{x_1 \in \chi_{1,c_{k'}}^i} \left\{ \frac{1}{\left(|\rho_{12}|^2 \sigma_2^2 + \left|\mathbf{h}_1^\dagger \mathbf{p}_1\right|^2 N_0\right)} \left| \overline{y}_1 - \left|\mathbf{h}_1^\dagger \mathbf{p}_1\right|^2 x_1 \right|^2 \right\} \tag{18}$$

Table 1 compares the complexities of different receivers in terms of the number of real-valued multiplications and additions for getting all LLR values per RE/subcarrier. Note that n_r denotes the number of receive antennas. This complexity analysis is independent of the number of transmit antennas as the operation of finding effective channels bears same

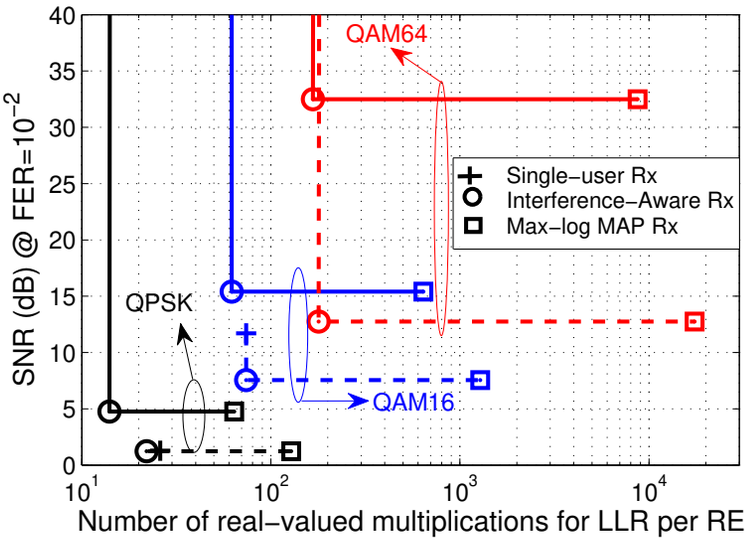

Figure 2. eNodeB has two antennas. Continuous lines indicate the case of single-antenna UEs while dashed lines indicate dual-antenna UEs. 3GPP LTE rate 1/2 punctured turbo code is used. Simulation settings are same as in the first part of Sec.7.

Receiver	Real Multiplications	Real Additions
Interference-aware receiver (Equal energy alphabets)	$8n_r + 2\sqrt{M} + 2M$	$8n_r + 10M + \log(M) - 4$
Interference-aware receiver (Non Equal energy alphabets)	$12n_r + 4M + \frac{7}{2}\sqrt{M}$	$12n_r + 18M + \log(M) - 6$
Max-log MAP receiver	$2M^2n_r + 8Mn_r$	$6M^2n_r + 4Mn_r + \log(M) - M^2$
Single-user receiver (Equal energy alphabets)	$10n_r + 6$	$10n_r - 3$
Single-user receiver (Non Equal energy alphabets)	$10n_r + 3M + \sqrt{M}/2 + 4$	$10n_r + 3M + \log(M) - 3$

Table 1. Comparison of receivers complexity

complexity in all receiver structures. Moreover UEs can also directly estimate their effective channels if the pilot signals are also precoded. The comparison shows that the complexity of the interference-aware receiver is of the same order as of single-user receiver while it is far less than the complexity of the max log MAP receiver. Fig. 2 further shows the performance-complexity trade off of different receivers for multi-user MIMO mode in LTE. The performance of the receivers is measured in terms of the SNR at the frame error rate (FER) of 10^{-2} whereas the complexity is determined from Table.1. It shows that the performance of the single-user receiver is severely degraded as compared to that of the interference-aware receiver. In most cases, the single-user receiver fails to achieve the requisite FER in the considered SNR range. On the other hand, interference-aware receiver achieves same performance as max log MAP receiver but with much reduced complexity.

The interference-aware receiver is therefore not only characterized by low complexity but it also resorts to intelligent detection by exploiting the structure of residual interference. Moreover, this receiver structure being based on the MF outputs and devoid of any division operation can be easily implemented in the existing hardware. However the proposed receiver needs both the channel knowledge and the constellation of interference (co-scheduled UE). As the UE already knows its own channel from the eNodeB and the requested precoder, it can determine the effective channel of the interference based on the geometric scheduling algorithm, i.e. the precoder of the co-scheduled UE is 180° out of phase of its own precoder. Consequently there is no additional complexity in utilizing this receiver

http://dx.doi.org/10.5772/57134

structure as compared to using single-user receivers except that the UE needs to know the constellation of interference.

4. Information theoretic perspective

Sum rate of the downlink channel is given as

$$\mathcal{I} = I\left(Y_1; X_1 \middle| \mathbf{h}_1^\dagger, \mathbf{P}\right) + I\left(Y_2; X_2 \middle| \mathbf{h}_2^\dagger, \mathbf{P}\right) \tag{19}$$

where $\mathbf{P} = [\mathbf{p}_1\ \mathbf{p}_2]$ is the precoder matrix, $I\left(Y_1; X_1 \middle| \mathbf{h}_1^\dagger, \mathbf{P}\right)$ is the mutual information of UE-1 once it sees interference from UE-2 and $I\left(Y_2; X_2 \middle| \mathbf{h}_2^\dagger, \mathbf{P}\right)$ is the mutual information of UE-2 once it sees interference from UE-1. Note that Y_1 is the received symbol at UE-1 while X_1 is the symbol transmitted by the eNodeB to UE-1. Note that interference is present in the statistics of Y_1 and Y_2. No sophisticated power allocation is employed to the two streams as the downlink control information (DCI) in the multi-user mode in LTE includes only 1-bit power offset information, indicating whether a 3 dB transmit power reduction should be assumed or not. We therefore consider equal-power distribution between the two streams. For the calculation of mutual information, we deviate from the unrealistic Gaussian assumption for the alphabets and consider them from discrete constellations. The derivations of the mutual information expressions for the case of finite alphabets have been relegated to Appendix-A for simplicity and lucidity.

We focus on the LTE precoders but to analyze the degradation caused by the low-level quantization and the characteristic of EGT of these precoders, we also consider some other transmission strategies. Firstly we consider unquantized MF precoder [27] which is given as

$$\mathbf{p} = \frac{1}{\sqrt{|h_{11}|^2 + |h_{21}|^2}} \begin{bmatrix} h_{11} \\ h_{21} \end{bmatrix} \tag{20}$$

For EGT, the unquantized MF precoder is given as

$$\mathbf{p} = \frac{1}{\sqrt{2}} \begin{bmatrix} 1 \\ h_{11}^* h_{21} / \left|h_{11}\right| \left|h_{21}\right| \end{bmatrix} \tag{21}$$

To be fair in comparison with the geometric scheduling algorithm for multi-user MIMO in LTE, we introduce a geometric scheduling algorithm for unquantized precoders. We divide the spatial space into 4 quadrants according to the spatial angle between $\mathbf{h}_1^\dagger$ and $\mathbf{h}_2^\dagger$ which is given as

$$\phi = \cos^{-1}\left(\frac{\left|\mathbf{h}_1^\dagger \mathbf{h}_2\right|}{\|\mathbf{h}_1\| \, \|\mathbf{h}_2\|}\right) \qquad 0^\circ \leq \phi \leq 90^\circ \tag{22}$$

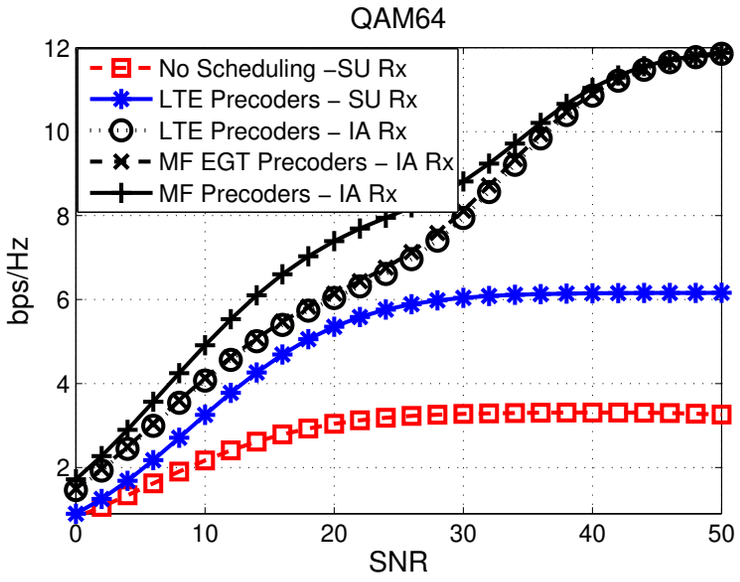

Figure 3. Sum rates of different transmission schemes for the downlink channel with dual-antenna eNodeB and 2 single-antenna UEs. 'No Scheduling - SU Rx' indicates the case once the eNodeB uses the LTE precoders without employing the geometric scheduling strategy. In all other cases, the eNodeB employs the geometric scheduling strategy along with the LTE precoders, MF EGT precoders and MF precoders. SU Rx indicates the cases when UEs employ single-user detection while IA Rx indicates the cases when UEs resort to the intelligent detection by employing the low-complexity interference-aware receivers.

The geometric scheduling algorithm ensures that the eNodeB chooses the second UE to be served on the same RE as the first UE such that their channels $\mathbf{h}_1^\dagger$ and $\mathbf{h}_2^\dagger$ lie in the opposite quadrants.

Fig. 3 shows the sum rates of a broadcast channel with the dual-antenna eNodeB and 2 single-antenna UEs for QAM64 alphabets. SNR is the transmit SNR, i.e. $\frac{\sigma_1^2\|\mathbf{p}_1\|^2+\sigma_2^2\|\mathbf{p}_2\|^2}{N_0}$ whereas the two UEs have equal power distribution, i.e. $\sigma_1^2 = \sigma_2^2$. MF and MF EGT precoders are the unquantized precoders given in (20) and (21) respectively while LTE precoders are the quantized precoders given in (1). The sum rates of unquantized precoders along with those of LTE quantized precoders are shown for the case of single-user receivers and for the case of low-complexity interference-aware receivers. The results show that under the proposed transmission strategy, the sum rate can be significantly improved (unbounded in SNR) if the low-complexity interference-aware receivers are used as compared to the case when the UEs resort to sub-optimal single-user detection where rates are bounded (in SNR). The behavior of single-user detection is attributed to the fact that this detection strategy considers interference as noise so the SINR is low once no geometric scheduling has been employed by the eNodeB while the SINR improves due to the reduction of interference once geometric scheduling is employed. However the rates remain bounded in the SNR if the UEs resort to the single-user detection which is due to the fact that increasing the SNR (transmit SNR) also increases the interference strength thereby bounding the SINR at high values of the transmit SNR. On the other hand, there is significant improvement in the sum rate once UEs resort to intelligent detection by employing the low-complexity interference-aware receivers. In this case, the sum rate is unbounded if the rate (constellation size) of each UE is adapted with the SNR. Note that the quantized CSIT (LTE precoders) appears to have no effect at high SNR once UEs resort to intelligent interference-aware detection. This behavior is because the

http://dx.doi.org/10.5772/57134

rate is not adapted with the SNR in these simulations, i.e. the constellation size is fixed to QAM64 and is not increased with the increase in the SNR. At high SNR, the rate of each UE gets saturated to its constellation size (6 bits for QAM64) if the UE resorts to intelligent interference-aware detection. However the approach to this saturation point (slope of the rate curve) depends on the quantization of channel information.

Another interesting result is the effect of the two characteristics of LTE precoders, i.e. low-resolution and EGT. There is a slight improvement in the sum rate at medium SNR when the restriction of low-resolution (LTE quantized precoders) is relaxed, i.e. eNodeB employs MF EGT precoders however there is a significant improvement in the sum rate when the restriction of EGT is eliminated, i.e the eNodeB employs MF precoders. This shows that the loss in spectral efficiency due to the employment of LTE precoders is mainly attributed to the EGT rather than their low resolution (quantization).

5. Performance analysis

We now focus on the EGT characteristic of the LTE precoders and carry out the performance analysis of the EGT in single-user and multi-user MIMO systems. We restrict to the case of single-antenna UEs while the eNodeB has two antennas.

5.1. Single-user MIMO

For the single-user case, the received signal at the k-th RE is given by

$$y_{1,k} = \mathbf{h}_{1,k}^{\dagger}\mathbf{p}_{1,k}x_{1,k} + z_{1,k} \tag{23}$$

For EGT, the precoder vector is given by $\mathbf{p}_{1,k} = \frac{1}{\sqrt{2}}\begin{bmatrix}1 & \frac{h_{21,k}h_{11,k}^{*}}{|h_{21,k}||h_{11,k}|}\end{bmatrix}^{T}$. So the received signal after normalization by $\frac{h_{11,k}}{|h_{11,k}|}$ is given by

$$y_{1,k}^{N} = \frac{1}{\sqrt{2}}\left(|h_{11,k}| + |h_{21,k}|\right)x_{1,k} + \frac{h_{11,k}}{|h_{11,k}|}z_{1,k} \tag{24}$$

where $y_{1,k}^{N} = \frac{h_{11,k}}{|h_{11,k}|}y_{1,k}$. The max log MAP bit metric [4] for the bit $c_{k'}$ can be written as

$$\Lambda_1^i\left(y_k, c_{k'}\right) \approx \min_{x_1 \in \chi_{1,c_{k'}}^{i}} \left[\frac{1}{N_0}\left|y_{1,k}^{N} - \frac{1}{\sqrt{2}}\left(|h_{11,k}| + |h_{21,k}|\right)x_1\right|^2\right] \tag{25}$$

The conditional PEP i.e $P\left(\underline{\mathbf{c}}_1 \rightarrow \hat{\underline{\mathbf{c}}}_1 | \mathbf{h}_1\right)$ is given as

$$P\left(\underline{\mathbf{c}}_1 \rightarrow \hat{\underline{\mathbf{c}}}_1|\overline{\mathbf{H}}_1\right) = P\left(\sum_{k'} \min_{x_1 \in \chi^i_{1,c_{k'}}} \frac{1}{N_0}\left|y^N_{1,k} - \frac{1}{\sqrt{2}}\left(|h_{11,k}| + |h_{21,k}|\right)x_1\right|^2 \right.$$
$$\left. \geq \sum_{k'} \min_{x_1 \in \chi^i_{1,\hat{c}_{k'}}} \frac{1}{N_0}\left|y^N_{1,k} - \frac{1}{\sqrt{2}}\left(|h_{11,k}| + |h_{21,k}|\right)x_1\right|^2 \left|\overline{\mathbf{H}}_1\right.\right) \tag{26}$$

where $\overline{\mathbf{H}}_1$ indicates the complete channel from the eNodeB to UE-1 for the transmission of the codeword $\underline{\mathbf{c}}_1$. Assume $d\left(\underline{\mathbf{c}}_1 - \hat{\underline{\mathbf{c}}}_1\right) = d_{free}$ for $\underline{\mathbf{c}}_1$ and $\hat{\underline{\mathbf{c}}}_1$ under consideration for the PEP analysis, which is the worst case scenario between any two codewords. Therefore, the inequality on the right hand side of (26) shares the same terms on all but d_{free} summation points and the summations can be simplified to only d_{free} terms for which $\hat{c}_{k'} = \bar{c}_{k'}$. Let's denote

$$\tilde{x}_{1,k} = \arg \min_{x_1 \in \chi^i_{1,c_{k'}}} \frac{1}{N_0}\left|y^N_{1,k} - \frac{1}{\sqrt{2}}\left(|h_{11,k}| + |h_{21,k}|\right)x_1\right|^2$$
$$\hat{x}_{1,k} = \arg \min_{x_1 \in \chi^i_{1,\bar{c}_{k'}}} \frac{1}{N_0}\left|y^N_{1,k} - \frac{1}{\sqrt{2}}\left(|h_{11,k}| + |h_{21,k}|\right)x_1\right|^2 \tag{27}$$

As $\frac{1}{N_0}\left|y^N_{1,k} - \frac{1}{\sqrt{2}}\left(|h_{11,k}| + |h_{21,k}|\right)x_{1,k}\right|^2 \geq \frac{1}{N_0}\left|y^N_{1,k} - \frac{1}{\sqrt{2}}\left(|h_{11,k}| + |h_{21,k}|\right)\tilde{x}_{1,k}\right|^2$, this leads to PEP being given as

$$P\left(\underline{\mathbf{c}}_1 \rightarrow \hat{\underline{\mathbf{c}}}_1|\overline{\mathbf{H}}_1\right) \leq P\left(\sum_{k,d_{free}} \frac{1}{N_0}\left|y^N_{1,k} - \frac{1}{\sqrt{2}}\left(|h_{11,k}| + |h_{21,k}|\right)x_{1,k}\right|^2 \right.$$
$$\left. \geq \sum_{k,d_{free}} \frac{1}{N_0}\left|y^N_{1,k} - \frac{1}{\sqrt{2}}\left(|h_{11,k}| + |h_{21,k}|\right)\hat{x}_{1,k}\right|^2 \left|\overline{\mathbf{H}}_1\right.\right) \tag{28}$$
$$= P\left(\sum_{k,d_{free}} \frac{\sqrt{2}\left(|h_{11,k}| + |h_{21,k}|\right)}{N_0}\left(z^*_{1,k}\left(\hat{x}_{1,k} - x_{1,k}\right)\right)_R \right.$$
$$\left. \geq \sum_{k,d_{free}} \frac{1}{2N_0}\left(|h_{11,k}| + |h_{21,k}|\right)^2 |\hat{x}_{1,k} - x_{1,k}|^2\right)$$
$$= Q\left(\sqrt{\sum_{k,d_{free}} \frac{1}{4N_0}\left(|h_{11,k}| + |h_{21,k}|\right)^2 |(x_{1,k} - \hat{x}_{1,k})|^2}\right)$$
$$\leq \frac{1}{2}\exp\left(-\sum_{k,d_{free}} \frac{1}{8N_0}\left(|h_{11,k}| + |h_{21,k}|\right)^2 d^2_{1,\min}\right)$$
$$= \frac{1}{2}\prod_{k,d_{free}} \exp\left(-\frac{1}{8N_0}\left(|h_{11,k}| + |h_{21,k}|\right)^2 d^2_{1,\min}\right) \tag{29}$$

http://dx.doi.org/10.5772/57134

where we have used Chernoff bound $Q(x) \leq \frac{1}{2}\exp\left(\frac{-x^2}{2}\right)$. Averaging over channel leads to

$$P(\underline{\mathbf{c}}_1 \to \hat{\underline{\mathbf{c}}}_1) \leq \frac{1}{2} E_{\overline{\mathbf{H}}_1} \prod_{k,d_{free}} \exp\left(-\frac{1}{8N_0}\left(|h_{11,k}| + |h_{21,k}|\right)^2 d_{1,\min}^2\right)$$
$$= \frac{1}{2} \prod_{k,d_{free}} E_{\mathbf{h}_{1,k}} \exp\left(\left(-\frac{\breve{d}_{1,\min}^2}{4}\right) \frac{\left(|h_{11,k}| + |h_{21,k}|\right)^2 \sigma_1^2}{2N_0}\right) \quad (30)$$

(30) follows from the channel independence at each RE which is the consequence of the interleaving operation. Here we have used the notation $d_{1,\min}^2 = \sigma_1^2 \breve{d}_{1,\min}^2$ with $\breve{d}_{1,\min}^2$ being the normalized minimum distance of the constellation χ_1. Using the moment generating function (MGF) of the SNR at the output of two branch EGC as per equations (2) and (23) in [21], PEP at high SNR is upper bounded as

$$P(\underline{\mathbf{c}}_1 \to \hat{\underline{\mathbf{c}}}_1) \leq \frac{1}{2} \prod_{d_{free}} \left(\frac{8\left(\frac{\sigma_1^2}{N_0}\right)^2 + \breve{d}_{1,\min}^2 \left(\frac{\sigma_1^2}{N_0}\right)^3}{4\left(\frac{\sigma_1^2}{N_0}\right)^2 \left(2 + \frac{\sigma_1^2 \breve{d}_{1,\min}^2}{4N_0}\right)^2} - \frac{\left(\frac{\breve{d}_{1,\min}^2}{2\sqrt{2}}\right)\left(\frac{\sigma_1^2}{N_0}\right)}{\left(2 + \frac{\breve{d}_{1,\min}^2}{2}\left(\frac{\sigma_1^2}{N_0}\right)\right)^{3/2}} \right.$$
$$\times \left[\pi - 2\sin^{-1}\left(\sqrt{\frac{\left(\frac{\sigma_1^2}{N_0}\right)^{-1} + \frac{\breve{d}_{1,\min}^2}{4}}{2\left(\frac{\sigma_1^2}{N_0}\right)^{-1} + \frac{\breve{d}_{1,\min}^2}{4}}}\right)\right]$$
$$\left. + \frac{4\left(\frac{\sigma_1^2}{N_0}\right)^2 \left(4 + \frac{\breve{d}_{1,\min}^2}{2}\left(\frac{\sigma_1^2}{N_0}\right)\right)}{4\left(\frac{\sigma_1^2}{N_0}\right)^2 \left(2 + \frac{\breve{d}_{1,\min}^2}{4}\left(\frac{\sigma_1^2}{N_0}\right)\right)^2 \left(2 + \frac{\breve{d}_{1,\min}^2}{2}\left(\frac{\sigma_1^2}{N_0}\right)\right)} \right) \quad (31)$$

Using the identity $\cos^{-1}(x) = \frac{\pi}{2} - \sin^{-1}(x)$, we have

$$\pi - 2\sin^{-1}\left(\sqrt{\frac{\left(\frac{\sigma_1^2}{N_0}\right)^{-1} + \frac{\breve{d}_{1,\min}^2}{4}}{2\left(\frac{\sigma_1^2}{N_0}\right)^{-1} + \frac{\breve{d}_{1,\min}^2}{4}}}\right) = 2\cos^{-1}\left(\sqrt{\frac{\left(\frac{\sigma_1^2}{N_0}\right)^{-1} + \frac{\breve{d}_{1,\min}^2}{4}}{2\left(\frac{\sigma_1^2}{N_0}\right)^{-1} + \frac{\breve{d}_{1,\min}^2}{4}}}\right) \quad (32)$$

Taylor series expansion [10] of $\cos^{-1}\left(\sqrt{x}\right)$ is given as

$$\cos^{-1}\left(\sqrt{x}\right) = \sqrt{2-2\sqrt{x}}\sum_{k=0}^{\infty}\frac{\left(1-\sqrt{x}\right)^{k}(1/2)_{k}}{2^{k}\left(k!+2kk!\right)} \qquad \text{for } \left|-1+\sqrt{x}\right|<2$$

where $x!$ is the factorial of x while $(x)_n$ is the Pochhammer symbol, i.e. $(x)_n = x(x+1)\cdots(x+n-1)$. For x closer to 1, a case that shall be occurring at high SNR in (32), first term will be dominant, i.e.

$$\cos^{-1}\left(\sqrt{\frac{\left(\frac{\sigma_1^2}{N_0}\right)^{-1}+\frac{\check{d}_{1,\min}^2}{4}}{2\left(\frac{\sigma_1^2}{N_0}\right)^{-1}+\frac{\check{d}_{1,\min}^2}{4}}}\right) \approx \sqrt{2-2\sqrt{\frac{\left(\frac{\sigma_1^2}{N_0}\right)^{-1}+\frac{\check{d}_{1,\min}^2}{4}}{2\left(\frac{\sigma_1^2}{N_0}\right)^{-1}+\frac{\check{d}_{1,\min}^2}{4}}}} \tag{33}$$

Taylor series expansion of $\sqrt{x}$ at $x=1$ is

$$\sqrt{x} = 1+\frac{x-1}{2}-\frac{(x-1)^2}{8}+\frac{(x-1)^3}{16}-\cdots$$

In the expansion of $\sqrt{\frac{\left(\frac{\sigma_1^2}{N_0}\right)^{-1}+\frac{\check{d}_{1,\min}^2}{4}}{2\left(\frac{\sigma_1^2}{N_0}\right)^{-1}+\frac{\check{d}_{1,\min}^2}{4}}}$, first two terms will be dominant at high SNR thereby leading to

$$\begin{aligned}\sqrt{2-\sqrt{\frac{\left(\frac{\sigma_1^2}{N_0}\right)^{-1}+\frac{\check{d}_{1,\min}^2}{4}}{2\left(\frac{\sigma_1^2}{N_0}\right)^{-1}+\frac{\check{d}_{1,\min}^2}{4}}}} &\approx \sqrt{2-2\left(1+\frac{\frac{\left(\frac{\sigma_1^2}{N_0}\right)^{-1}+\frac{\check{d}_{1,\min}^2}{4}}{2\left(\frac{\sigma_1^2}{N_0}\right)^{-1}+\frac{\check{d}_{1,\min}^2}{4}}-1}{2}\right)} \\ &= \sqrt{-\left(\frac{\left(\frac{\sigma_1^2}{N_0}\right)^{-1}+\frac{\check{d}_{1,\min}^2}{4}}{2\left(\frac{\sigma_1^2}{N_0}\right)^{-1}+\frac{\check{d}_{1,\min}^2}{4}}-1\right)} \\ &= \frac{1}{\sqrt{2+\frac{\check{d}_{1,\min}^2}{4}\left(\frac{\sigma_1^2}{N_0}\right)}}\end{aligned} \tag{34}$$

So rewriting (31), we get

http://dx.doi.org/10.5772/57134

$$P\left(\underline{\mathbf{c}}_1 \rightarrow \hat{\underline{\mathbf{c}}}_1\right) \leq \frac{1}{2}\prod_{d_{free}}\left(\frac{2}{\left(2+\frac{\breve{d}^2_{1,\min}}{4}\left(\frac{\sigma_1^2}{N_0}\right)\right)^2}+\frac{\breve{d}^2_{1,\min}\left(\frac{\sigma_1^2}{N_0}\right)}{4\left(2+\frac{\breve{d}^2_{1,\min}}{4}\left(\frac{\sigma_1^2}{N_0}\right)\right)^2}\right.$$
$$-\frac{2\left(\frac{\breve{d}^2_{1,\min}}{2\sqrt{2}}\right)\left(\frac{\sigma_1^2}{N_0}\right)}{\left(2+\frac{\breve{d}^2_{1,\min}}{2}\left(\frac{\sigma_1^2}{N_0}\right)\right)^{3/2}\left(2+\frac{\breve{d}^2_{1,\min}}{4}\left(\frac{\sigma_1^2}{N_0}\right)\right)^{1/2}}$$
$$\left.+\frac{\left(4+\frac{\breve{d}^2_{1,\min}}{2}\left(\frac{\sigma_1^2}{N_0}\right)\right)}{\left(2+\frac{\breve{d}^2_{1,\min}}{4}\left(\frac{\sigma_1^2}{N_0}\right)\right)^2\left(2+\frac{\breve{d}^2_{1,\min}}{2}\left(\frac{\sigma_1^2}{N_0}\right)\right)}\right) \tag{35}$$

At high SNR, second term converges to $\frac{4}{\breve{d}^2_{1,\min}\left(\frac{\sigma_1^2}{N_0}\right)}$ while the third term converges to $\frac{-4}{\breve{d}^2_{1,\min}\left(\frac{\sigma_1^2}{N_0}\right)}$. So PEP at high SNR is upper bounded as

$$P\left(\underline{\mathbf{c}}_1 \rightarrow \hat{\underline{\mathbf{c}}}_1\right) \leq \frac{1}{2}\prod_{d_{free}}\left(\frac{32}{\left(\breve{d}^2_{1,\min}\left(\frac{\sigma_1^2}{N_0}\right)\right)^2}+\frac{16}{\left(\breve{d}^2_{1,\min}\left(\frac{\sigma_1^2}{N_0}\right)\right)^2}\right)$$
$$=\frac{1}{2}\prod_{d_{free}}\left(\frac{48}{\left(\breve{d}^2_{1,\min}\left(\frac{\sigma_1^2}{N_0}\right)\right)^2}\right) \tag{36}$$

where $\breve{d}^2_{1,\min}$ is the normalized minimum distance of the constellation χ_1, d_{free} is the free distance (minimum Hamming distance) of the code. Note that $\underline{\mathbf{c}}_1$ and $\hat{\underline{\mathbf{c}}}_1$ are the correct and error codewords respectively. (36) clearly shows full diversity of the EGT for single-user MIMO.

We now consider another approach to analyze the diversity order of EGT in the single-user MIMO transmission mode. We now focus on equal energy alphabets and consider the case of slow fading channel, i.e. the channel remains constant for the duration of one codeword. Rewriting the metric (28) in vector formulation i.e.

$$\sum_{k,d_{free}}\left|y^N_{1,k}-\frac{1}{\sqrt{2}}\left(|h_{11,k}|+|h_{21,k}|\right)x_{1,k}\right|^2=\left\|\mathbf{y}^N_1-\frac{1}{\sqrt{2}}\left(|h_{11}|+|h_{21}|\right)\mathbf{x}_1\right\|^2$$

So conditional PEP is given as

$$\begin{aligned} P\left(\underline{\mathbf{c}}_1 \rightarrow \hat{\underline{\mathbf{c}}}_1 | \overline{\mathbf{H}}_1\right) &\leq P\left(\left\|\mathbf{y}_1^N - \frac{1}{\sqrt{2}}\left(|h_{11}|+|h_{21}|\right)\mathbf{x}_1\right\|^2 \geq \left\|\mathbf{y}_1^N - \frac{1}{\sqrt{2}}\left(|h_{11}|+|h_{21}|\right)\hat{\mathbf{x}}_1\right\|^2\right) \\ &= P\left(\Re\left(\left(\frac{1}{\sqrt{2}}\left(|h_{11}|+|h_{21}|\right)\mathbf{x}+\mathbf{z}_1\right)^{\dagger}\left(\mathbf{x}_1-\hat{\mathbf{x}}_1\right)\right) \leq 0\right) \\ &= P\left(\frac{1}{\sqrt{2}}\left(|h_{11}|+|h_{21}|\right)\left(\|\mathbf{x}_1\|^2 - \Re\left(\mathbf{x}_1^{\dagger}\hat{\mathbf{x}}_1\right)\right) + \Re\left(\mathbf{z}_1^{\dagger}\left(\mathbf{x}_1-\hat{\mathbf{x}}_1\right)\right) \leq 0\right) \end{aligned} \tag{37}$$

Using $\|\mathbf{x}_1 - \hat{\mathbf{x}}_1\|^2 = \|\mathbf{x}_1\|^2 + \|\hat{\mathbf{x}}_1\|^2 - 2\Re\left(\hat{\mathbf{x}}_1\mathbf{x}\right)$ we get

$$\begin{aligned} P\left(\underline{\mathbf{c}}_1 \rightarrow \hat{\underline{\mathbf{c}}}_1 | \overline{\mathbf{H}}_1\right) &\leq P\left(\left(|h_{11}|+|h_{21}|\right)\left(\frac{3}{2\sqrt{2}}\|\mathbf{x}_1\|^2 - \frac{1}{2\sqrt{2}}\|\mathbf{x}_1-\hat{\mathbf{x}}_1\|^2 + \frac{1}{2\sqrt{2}}\|\hat{\mathbf{x}}_1\|^2\right) + \Re\left(\mathbf{z}_1^{\dagger}\left(\mathbf{x}_1-\hat{\mathbf{x}}_1\right)\right) \leq 0\right) \\ &= P\left(\kappa\left(|h_{11}|+|h_{21}|\right) + z_1^{'} \leq 0\right) \end{aligned}$$

where $\kappa = \frac{3}{2\sqrt{2}}\|\mathbf{x}_1\|^2 - \frac{1}{2\sqrt{2}}\|\mathbf{x}_1 - \hat{\mathbf{x}}_1\|^2 + \frac{1}{2\sqrt{2}}\|\hat{\mathbf{x}}_1\|^2$. $z_1^{'} = \Re\left(\mathbf{z}_1^{\dagger}\left(\mathbf{x}_1 - \hat{\mathbf{x}}_1\right)\right)$ is circularly symmetric complex while Gaussian noise of variance $\frac{N_0}{2}\|\mathbf{x} - \hat{\mathbf{x}}_1\|^2$. So the PEP is upperbounded as

$$P\left(\underline{\mathbf{c}}_1 \rightarrow \hat{\underline{\mathbf{c}}}_1 | \overline{\mathbf{H}}_1\right) \leq P\left(\kappa\left(|h_{11}|+|h_{21}|\right) + z_1^{'} \leq 0\right) \tag{38}$$

As per ours notations, the decision variable γ as per (5) and (13) in [29] is given as

$$\gamma = \kappa\left(|h_{11}|+|h_{21}|\right) + z_1^{'} \tag{39}$$

So the probability of error which is given as $P\left(\gamma \leq 0\right)$ is given as

$$P\left(\underline{\mathbf{c}}_1 \rightarrow \hat{\underline{\mathbf{c}}}_1\right) = \frac{1}{2}\left\{1 - \frac{\sqrt{\rho_{11}\left(\rho_{11}+2\kappa\right)} + \sqrt{\rho_{21}\left(\rho_{21}+2\kappa\right)}}{\rho_{11}+\rho_{21}+2\kappa}\right\} \tag{40}$$

where $\rho_{ij} = \mathbb{E}\left(\left|h_{ij}\right|^2\right)/N_0$ is the SNR at the individual branch and κ is a constant that will depend on the constellation. (40) shows the full diversity order of 2, a result earlier derived for EGT in single-user MIMO systems in [14] using the approach of metrics of diversity order.

http://dx.doi.org/10.5772/57134

5.2. Multi-user MIMO

We now focus on the PEP of UE-1 in the multi-user MIMO mode as per system equation (3). Let $\mathbf{p}_1 = [1 \;\; q]^T$ where $q \in \{\pm 1, \; \pm j\}$. To have good channel separation between the UEs to be served in the multi-user MIMO mode [8], scheduling at the eNodeB would ensure $\mathbf{p}_2$ to be $[1 \;\; -q]^T$. The effective channel seen by the desired stream $x_{1,k}$ at UE-1 is given as $h_{1,k} = h^*_{11,k} + qh^*_{21,k}$ whereas the channel seen by the interference stream $x_{2,k}$ is $h_{2,k} = h^*_{11,k} - qh^*_{21,k}$. The max log MAP bit metric is written as

$$\Lambda_1^i\left(y_{1,k}, c_{k'}\right) \approx \min_{x_1 \in \chi^i_{1,c_{k'}}, x_2 \in \chi_2} \frac{1}{N_0} \left| y_{1,k} - \frac{1}{\sqrt{4}} h_{1,k} x_1 - \frac{1}{\sqrt{4}} h_{2,k} x_2 \right|^2$$

Conditional PEP is given as

$$\begin{aligned} P\left(\underline{\mathbf{c}}_1 \to \hat{\underline{\mathbf{c}}}_1 | \overline{\mathbf{H}}_1\right) &= P\left(\sum_{k'} \min_{x_1 \in \chi^i_{1,c_{k'}}, x_2 \in \chi_2} \frac{1}{N_0} \left| y_{1,k} - \frac{1}{\sqrt{4}} h_{1,k} x_1 - \frac{1}{\sqrt{4}} h_{2,k} x_2 \right|^2 \right. \\ &\left. \geq \sum_{k'} \min_{x_1 \in \chi^i_{1,\hat{c}_{k'}}, x_2 \in \chi_2} \frac{1}{N_0} \left| y_{1,k} - \frac{1}{\sqrt{4}} h_{1,k} x_1 - \frac{1}{\sqrt{4}} h_{2,k} x_2 \right|^2 \right) \end{aligned} \tag{41}$$

Let's denote

$$\begin{aligned} \tilde{x}_{1,k}, \tilde{x}_{2,k} &= \arg \min_{x_1 \in \chi^i_{1,c_{k'}}, x_2 \in \chi_2} \frac{1}{N_0} \left| y_{1,k} - \frac{1}{\sqrt{4}} h_{1,k} x_1 - \frac{1}{\sqrt{4}} h_{2,k} x_2 \right|^2 \\ \hat{x}_{1,k}, \hat{x}_{2,k} &= \arg \min_{x_1 \in \chi^i_{1,\bar{c}_{k'}}, x_2 \in \chi_2} \frac{1}{N_0} \left| y_{1,k} - \frac{1}{\sqrt{4}} h_{1,k} x_1 - \frac{1}{\sqrt{4}} h_{2,k} x_2 \right|^2 \end{aligned} \tag{42}$$

Note that

$$\left| y_{1,k} - \frac{1}{\sqrt{4}} \left(h_{1,k} x_{1,k} + h_{2,k} x_{2,k} \right) \right|^2 \geq \left| y_{1,k} - \frac{1}{\sqrt{4}} \left(h_{1,k} \tilde{x}_{1,k} + h_{2,k} \tilde{x}_{2,k} \right) \right|^2$$

So conditional PEP is given as

$$\begin{aligned} P\left(\underline{\mathbf{c}}_1 \to \hat{\underline{\mathbf{c}}}_1 | \overline{\mathbf{H}}_1\right) &\leq Q\left(\sqrt{ \sum_{k, d_{free}} \frac{1}{8N_0} \left| h_{1,k} \left(x_{1,k} - \hat{x}_{1,k} \right) + h_{2,k} \left(x_{2,k} - \hat{x}_{2,k} \right) \right|^2 } \right) \\ &= Q\left(\sqrt{ \sum_{k, d_{free}} \frac{1}{8N_0} \left| \mathbf{h}_k^T \left(\mathbf{x}_k - \hat{\mathbf{x}}_k \right) \right|^2 } \right) \end{aligned} \tag{43}$$

where $\mathbf{h}_k = \begin{bmatrix} h_{11,k}^* & qh_{21,k}^* & h_{11,k}^* & -qh_{21,k}^* \end{bmatrix}^T$, $\mathbf{x}_k = \begin{bmatrix} x_{1,k} & x_{1,k} & x_{2,k} & x_{2,k} \end{bmatrix}^T$ and $\hat{\mathbf{x}}_k = \begin{bmatrix} \hat{x}_{1,k} & \hat{x}_{1,k} & \hat{x}_{2,k} & \hat{x}_{2,k} \end{bmatrix}^T$. We assume channel to be slow fading, i.e. the channel remains constant for the duration of one codeword. So the PEP can be written as

$$P\left(\underline{\mathbf{c}}_1 \to \hat{\underline{\mathbf{c}}}_1 | \overline{\mathbf{H}}_1\right) \leq Q\left(\sqrt{\sum_{k,d_{free}} \frac{1}{8N_0} \left|\mathbf{h}^T\left(\mathbf{x}_k - \hat{\mathbf{x}}_k\right)\right|^2}\right) = Q\left(\sqrt{\frac{1}{8N_0}\mathbf{h}^\dagger \mathbf{\Delta}\mathbf{\Delta}^\dagger \mathbf{h}}\right) \tag{44}$$

where $\mathbf{\Delta}\mathbf{\Delta}^\dagger$ is a 4×4 matrix while $\mathbf{\Delta}_{4\times d_{free}} = \left[\mathbf{x}_1 - \hat{\mathbf{x}}_1 \; \mathbf{x}_2 - \hat{\mathbf{x}}_2 \; \cdots \; \mathbf{x}_{k,d_{free}} - \hat{\mathbf{x}}_{k,d_{free}}\right]$. Using Chernoff bound, (44) is upper bounded by

$$P\left(\mathbf{c}_1 \to \hat{\mathbf{c}}_1 | \mathbf{h}\right) \leq \frac{1}{2} \exp\left(-\frac{1}{16N_0}\mathbf{h}^\dagger \mathbf{\Delta}\mathbf{\Delta}^\dagger \mathbf{h}\right) \tag{45}$$

The covariance matrix of the channel $\mathbf{h}$ is

$$E\left[\mathbf{h}\mathbf{h}^\dagger\right] = \mathbf{R} = \begin{bmatrix} 1 & 0 & 1 & 0 \\ 0 & 1 & 0 & -1 \\ 1 & 0 & 1 & 0 \\ 0 & -1 & 0 & 1 \end{bmatrix} \tag{46}$$

Its rank is two with its two identical eigenvalues being 2. Using the moment generating function of a Hermitian quadratic form in complex Gaussian random variable, we get

$$E_{\mathbf{h}}\left[\frac{1}{2}\exp\left(-\frac{1}{16N_0}\mathbf{h}^\dagger \mathbf{\Delta}\mathbf{\Delta}^\dagger \mathbf{h}\right)\right] \leq \frac{1}{2\det\left(\mathbf{I} + \frac{1}{16N_0}\mathbf{R}\mathbf{\Delta}\mathbf{\Delta}^\dagger\right)} \tag{47}$$

Note that the minimizations in (42) ensure that in $\mathbf{\Delta}$, $\hat{x}_{1,k}^{'} - x_{1,k}^{'}$ is always non-zero where $\hat{x}_{2,k}^{'} - x_{2,k}^{'}$ can be zero for $k = 1, \cdots, d_{free}$. So in the worst case scenario, $\mathbf{\Delta}$ would have only first two rows with non-zero elements. For the high SNR approximation, we get

$$P\left(\underline{\mathbf{c}}_1 \to \hat{\underline{\mathbf{c}}}_1\right) \leq \frac{1}{2}\left(\frac{16N_0}{\sigma^2}\right)^r \prod_{k=1}^{r} \frac{1}{\mu_k} \tag{48}$$

where r is the rank and μ_k are the eigenvalues of $\mathbf{R}\mathbf{\Delta}\mathbf{\Delta}^\dagger$. The minimum rank is one thereby indicating the diversity order of one. Note that as the derivation has involved Chernoff bound, so the exact PEP expression would involve some additional multiplicative factors but these factors will not affect the diversity order.

http://dx.doi.org/10.5772/57134

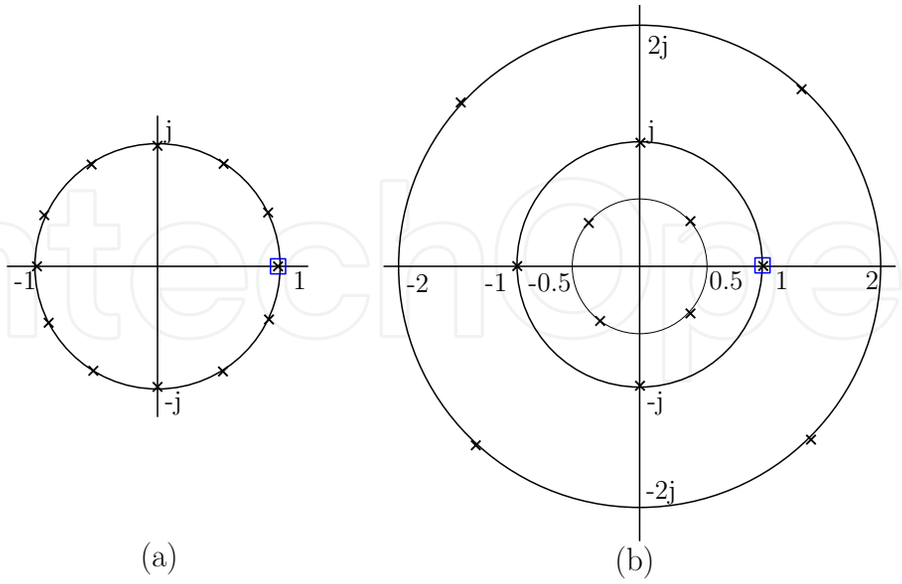

Figure 4. Two options of increasing the precoder codebook size. Fig.(a) corresponds to the option of increased angular resolution of LTE precoders while Fig.(b) corresponds to the option of enhanced levels of transmission. Square indicates the precoder entry for the first antenna while cross indicates the precoder entry for the second antenna.

6. The proposed feedback and codebook design

It was shown in the PEP analysis that the multi-user MIMO mode in LTE suffers from a loss of diversity. This loss is mainly attributed to the EGT characteristic of these precoders as will be shown in the next section. On the other hand, this transmission characteristic does not affect the diversity order in single-user MIMO mode. Focusing on this result, we propose a design of LTE precoders to offset this diversity loss.

LTE precoders are characterized by two features, i.e. angular resolution and EGT. Limited increase in the feedback can be either employed to increase the angular resolution of these structured precoders or it can be used to enhance the levels of transmission. Increasing the levels of transmission implies that additional feedback bits can be used to indicate an increase of the power level on either of the two antennas, i.e. creating more circles with different radii. For this we resorted to numerical optimization for fixing the radii of two circles and the precoders turn out to be $[1 \quad 2\exp(j\theta)]^T$ or $[2\exp(j\theta) \quad 1]^T$ where $\theta \in \{0, \pm 90^\circ, 180^\circ\}$. This approach gives 8 additional codebook entries, and 12 in total. Improving angular resolution is trivial, i.e. increasing equally angular spaced points on the unit circle but restricting to EGT, i.e. precoder is given as $[1 \quad \exp(j\theta)]^T$, where $\theta = 2\pi l/12, l = 0, \ldots, 11$. These two different codebook options have been illustrated in Fig. 4.

To quantize the proposed codebooks of size 12, $\lceil \log_2(12) \rceil = 4$ bits are needed. That means that we could add 4 more additional codebook entries for free, but it is not obvious how those extra entries should be designed in the case of the codebook with the additional transmission levels. On the other hand it can be argued that several PMI feedbacks (for example for different subbands) can be bundled to optimize the feedback rate.

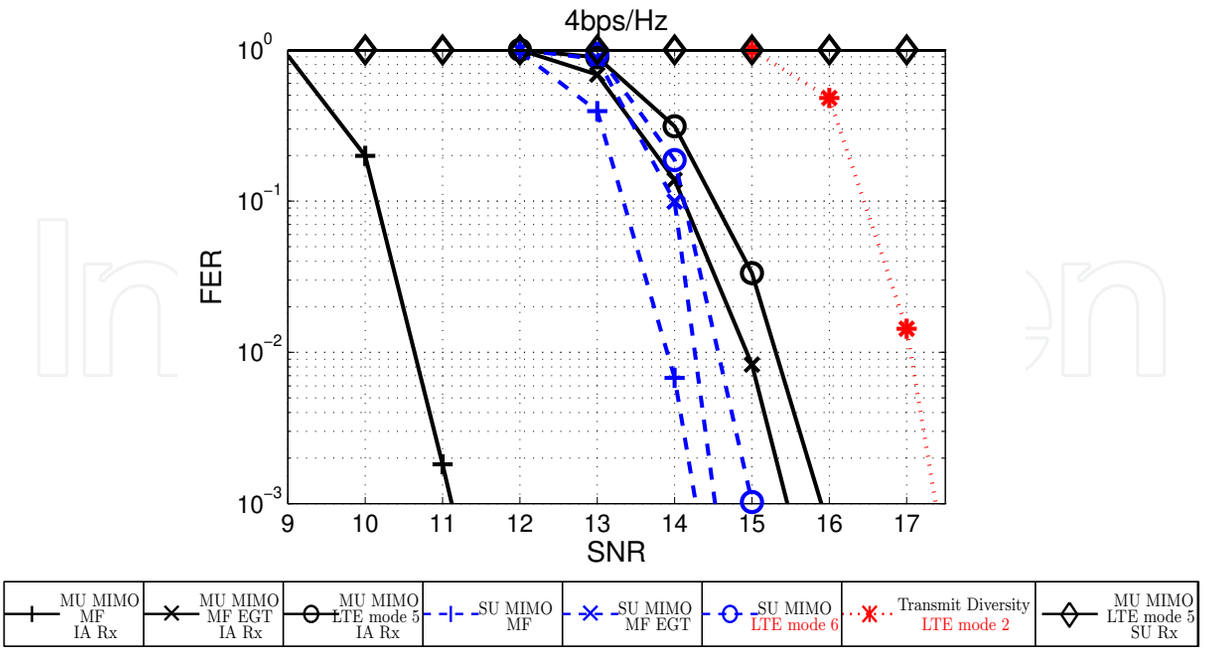

Figure 5. Downlink fast fading channel with the dual-antenna eNodeB and 2 single-antenna UEs. IA Rx indicates the low-complexity interference-aware receiver while SU Rx indicates the single-user receiver. MU MIMO and SU MIMO indicate multi-user and single-user MIMO respectively. To be fair in comparison amongst different schemes, sum rates are fixed, i.e. if 2 users are served with QPSK with rate 1/2 in the multi-user mode, then one user is served with QAM16 with rate 1/2 in the single-user mode thereby equating the sum rate in both cases to 2bps/Hz. 3GPP LTE rate 1/3 turbo code is used with different puncturing patterns.

7. Simulation results

Simulations are divided into 3 parts. In the first part, we look at the performance of the proposed interference-aware receiver structure for the multi-user MIMO mode in LTE while second part is dedicated to the sensitivity analysis of this receiver structure to the knowledge of the constellation of interference. This sensitivity analysis is motivated by the fact that the DCI formats in the transmission mode 5 (multi-user MIMO) do not include the information of the constellation of the co-scheduled UE. Third part looks at the diversity order of the EGT in both single-user and multi-user MIMO modes in LTE.

For the first part (Figs. 5 and 6), we consider the downlink of 3GPP LTE which is based on BICM OFDM transmission from the eNodeB equipped with two antennas using rate-1/3 LTE turbo code[1] [16] with rate matching to rate 1/2 and 1/4. We deliberate on both the cases of single and dual-antenna UEs. We consider an ideal OFDM system (no ISI) and analyze it in the frequency domain where the channel has iid Gaussian matrix entries with unit variance and is independently generated for each channel use. We assume no power control in the multi-user MIMO mode so two UEs have equal power distribution. Furthermore, all mappings of the coded bits to QAM symbols use Gray encoding. We focus on the FER while the frame length is fixed to 1056 information bits. As a reference, we consider the fall-back transmit diversity scheme (LTE mode 2 - Alamouti code) and compare it with the single-user and multi-user MIMO modes employing single-user receivers and

[1] The LTE turbo decoder design was performed using the coded modulation library www.iterativesolutions.com

http://dx.doi.org/10.5772/57134

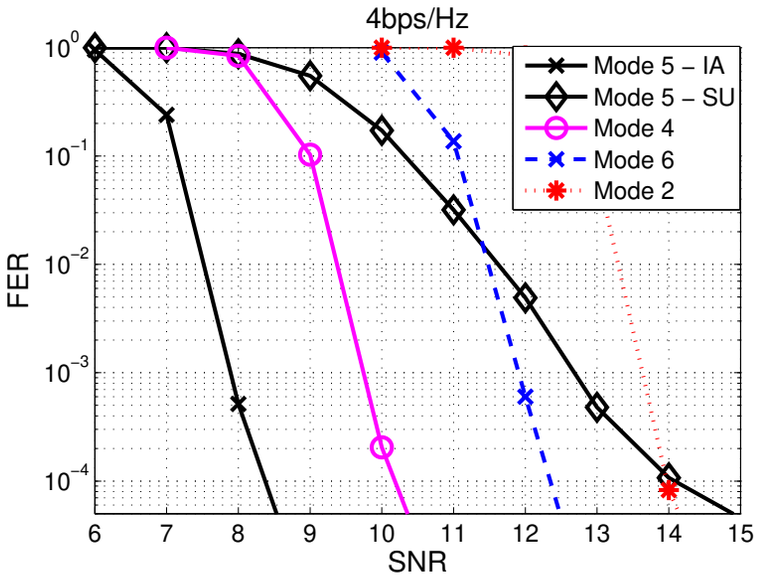

Figure 6. Downlink fast fading channel with the dual-antenna eNodeB and 2 dual-antenna UEs. IA indicates the low-complexity interference-aware receiver while SU indicates the single-user receiver. 3GPP LTE rate 1/3 turbo code is used with different puncturing patterns.

low-complexity interference-aware receivers. To analyze the degradation caused by the low-resolution and EGT of LTE precoders, we also look at the system performance employing the unquantized MF and unquantized MF EGT precoders. To be fair in the comparison of the LTE multi-user MIMO mode (mode 5) employing the geometric scheduling algorithm with the multi-user MIMO mode employing unquantized MF and MF EGT precoders, we consider the geometric scheduling algorithm (Section 4) based on the spatial angle between the two channels (equation (22)). Perfect CSIT is assumed for the case of MF and MF EGT precoding while error free feedback of 2 bits (PMI) to the eNodeB is assumed for LTE precoders. It is assumed that the UE has knowledge of the constellation of co-scheduled UE in the multi-user MIMO mode. It is further assumed that the UE knows its own channel from the eNodeB. So in multi-user MIMO mode, the UE can find the effective interference channel based on the fact that the eNodeB schedules the second UE on the same RE whose precoder is 180° out of phase of the precoder of the first UE. Fig. 5 shows the results for the case of single-antenna UEs. It shows enhanced performance of the multi-user MIMO mode once the UEs resort to intelligent detection by employing the low-complexity interference-aware receivers. The performance is severely degraded once the UEs resort to single-user detection. An interesting result is almost the equivalent performance of the unquantized MF EGT and low-resolution LTE precoders which shows that the loss with respect to the unquantized CSIT is attributed to the EGT rather than the low-resolution of LTE precoders.

Fig. 6 shows the results for the case of dual-antenna UEs and focuses on different LTE modes employing LTE precoders. It shows the degraded performance of single-user detection which is due to the fact that the rate with single-user detection gets saturated at high SNR due to the increased interference strength as was shown in Section. 4. So the performance of single-user detection is degraded as the spectral efficiency is higher than the rate or mutual information of the single-user detection. For single-user MIMO (Mode 6), there is no saturation of the rate at high SNR as there is no interference. So mode 6 performs better than mode 5 at

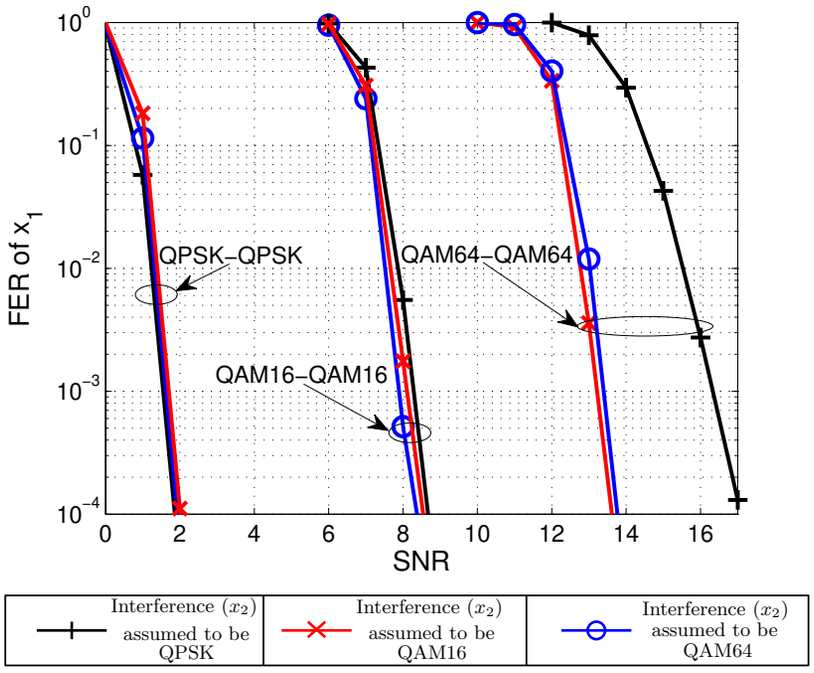

Figure 7. Interference sensitivity for the multi-user MIMO mode in LTE. Three sets of simulations are shown. QPSK-QPSK indicates that both x_1 and x_2 belong to QPSK. UE-1 does not know the constellation of interference (x_2) and assumes it to be QPSK, QAM16 and QAM64.

high SNR once UEs employ single-user detection. However if UEs resort to the intelligent interference-aware detection, the multi-user MIMO mode shows enhanced performance over other transmission modes in LTE. No degradation of LTE multi-user MIMO mode is observed at higher spectral efficiencies once UEs have receive diversity (dual antennas).

In the second part of simulations, we look at the sensitivity of the proposed receiver structure to the knowledge of the constellation of co-scheduled UE for the multi-user MIMO mode in LTE. The simulation settings are same as of the first part except that we consider the case when UE has no knowledge of the constellation of co-scheduled UE. The UE assumes this unknown interference constellation to be QPSK, QAM16 or QAM64 and the results for these different assumptions are shown in Fig. 7. Results show that there is negligible degradation in the performance of the proposed receiver if the interfering constellation is assumed to be QAM16 or QAM64. However, there is significant degradation if the interference is assumed to be QPSK when it actually comes from QAM64. It indicates that assuming interference to be from a higher order modulation amongst the possible modulation alphabets leads to the best compromise as this assumption includes the lower modulation orders as special cases (with proper scaling). However the converse is not true, i.e. assuming interference from lower modulation order cannot include higher order modulations. As LTE and LTE-Advanced restrict the transmission to three modulations (QPSK, QAM16 and QAM64), assuming interference to be QAM64 (or even QAM16) leads to better performance. If the interference constellation also includes QAM256, then assuming interference to be QAM256 (or even QAM64) would lead to better results. These results have not been shown here as LTE and LTE-Advanced do not support QAM256 modulation. The proposed receiver structure, therefore, can still exploit the discrete nature of the interference even if it does not know

http://dx.doi.org/10.5772/57134

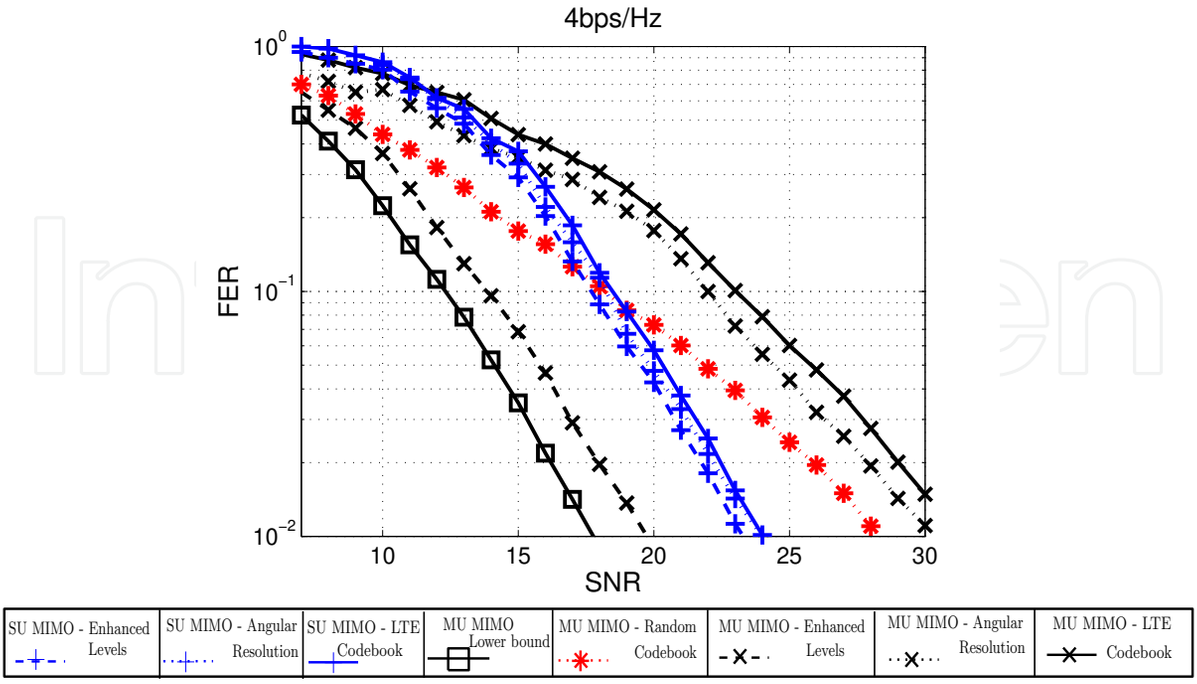

Figure 8. Proposed precoder codebook. Downlink channel with dual-antenna eNodeB and two single-antenna UEs. The figure illustrates the performance for the sum rate of 4bps/Hz. SNR is the transmit SNR while sum rate is same for single-user and multi-user MIMO, i.e. if two UEs are served with QPSK, rate 1/2, in multi-user mode, then one UE is served with QAM16, rate 1/2, in the single-user mode. SU MIMO and MU MIMO indicate single-user and multi-user MIMO.

its modulation order. As the complexity of this receiver structure is independent of the constellation of interference, the assumption of higher order modulation does not add to the complexity of detection.

In the third set of simulations, we look at the diversity order of the single-user MIMO and multi-user MIMO schemes in LTE. The system settings are same as in the first part but now we consider slow fading environment, i.e. the channel remains constant for the duration of one codeword. Fig. 8 shows significant improvement in the performance of the multi-user MIMO mode when additional codebook entries are employed to increase the levels of transmission as compared to the case of increasing the angular resolution of precoders. However creating two levels of transmission leads to significant improvement as the performance moves closer to the upper bound. This hypothetical upper bound is the performance curve for MF precoder in multi-user MIMO mode without any interference, i.e. the eNodeB serves two UEs with their respective MF based precoders and the two UEs do not see any interference. The change of the slope of FER curve with increased levels of transmission indicates improved diversity as compared to the case of increased angular resolution. On the other hand, little gain is observed in the single-user mode (LTE transmission mode 6) with additional codebook entries which is expected as the standard LTE precoders have been optimized for the single-user transmission [22]. For comparison purposes, we have also considered the case of random codebooks. The main advantage of random codebooks is that they indicate some sort of performance lower bound and with any intelligent feedback design, system is bound to perform better.

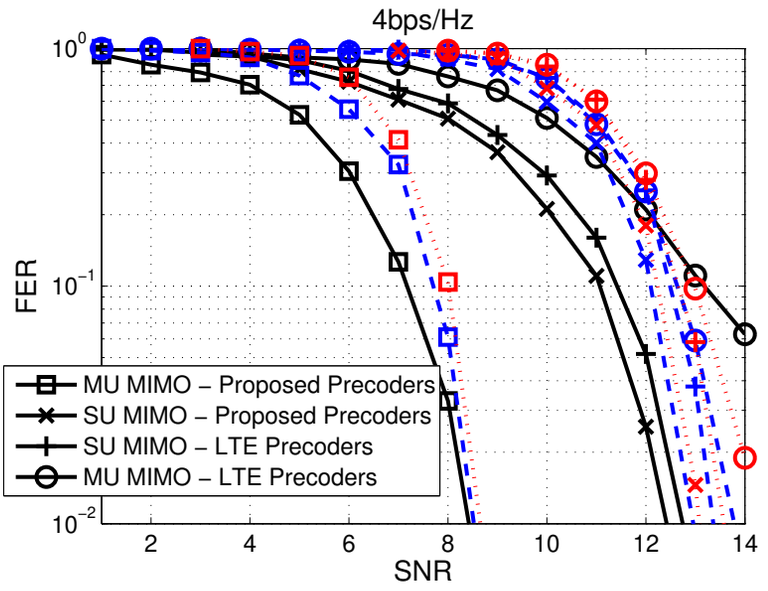

Figure 9. Performance of the proposed precoder codebook in 3GPP LTE channel models [18]. Black continuous lines show the Extended Pedestrian A model (EPA), blue dashed lines show Extended Vehicular A model (EVA), while red dotted lines show Extended Typical Urban model (ETU).

Fig. 9 shows the case where we have considered 3GPP LTE channel model introduced in [18] for three representative scenarios, i.e. pedestrian, vehicular and typical urban scenario. The transmission chain is dominantly LTE compliant with 15 KHz subcarrier-spacing and 20 MHz system bandwidth. The results confirm the earlier findings of the improved performance of proposed codebook design (enhanced levels of transmission) for multi-user transmission mode. Pedestrian channel offers less diversity in the channel as compared to the vehicular channel, so the performance of LTE precoders for multi-user MIMO in severely degraded in the former case. However as the proposed precoder design recovers the lost order of diversity, there is an improvement of 6dB at the target FER of 10^{-1}.

8. Conclusions

In this chapter, we have looked at the feasibility of the multi-user MIMO for future wireless systems which are characterized by low-level quantization of CSIT. We have shown that multi-user MIMO can deliver its promised gains if the UEs resort to intelligent detection rather than the sub-optimal single-user detection. To this end, we have proposed a low-complexity interference-aware receiver structure which is characterized by the exploitation of the structure of residual interference. We have further investigated the impact of low-level fixed rate feedback on the performance of multi-user MIMO in LTE systems. We have analyzed two important characteristics of the LTE precoders, i.e. low resolution and EGT. We have shown that the performance loss of the LTE precoders in the multi-user MIMO mode is attributed to their characteristic of EGT rather than their low resolution. We have proposed a feedback and precoding design and have shown that the performance in multi-user MIMO significantly improves once strategy of more levels of transmission is resorted to as compared to the case of increased angular resolution. The work presented in this chapter is not merely confined to the framework of LTE, rather it gives the receiver structure and precoding design guidelines for modern wireless systems.

http://dx.doi.org/10.5772/57134

Appendix A
Mutual information for finite alphabets

The mutual information for UE-1 for finite size QAM constellation with $|\chi_1| = M_1$ takes the form as

$$\begin{aligned} I\left(Y_1; X_1 | \mathbf{h}_1^\dagger, \mathbf{P}\right) &= \mathcal{H}\left(X_1 | \mathbf{h}_1^\dagger, \mathbf{P}\right) - \mathcal{H}\left(X_1 | Y_1, \mathbf{h}_1^\dagger, \mathbf{P}\right) \\ &= \log M_1 - \mathcal{H}\left(X_1 | Y_1, \mathbf{h}_1^\dagger, \mathbf{P}\right) \end{aligned} \tag{49}$$

where $\mathcal{H}(.) = -E \log p(.)$ is the entropy function. The second term of (49) is given as

$$\begin{aligned} \mathcal{H}\left(X_1 | Y_1, \mathbf{h}_1^\dagger, \mathbf{P}\right) &= \sum_{x_1} \int_{y_1} \int_{\mathbf{h}_1^\dagger \mathbf{p}_1} \int_{\mathbf{h}_1^\dagger \mathbf{p}_2} p\left(x_1, y_1, \mathbf{h}_1^\dagger \mathbf{p}_1, \mathbf{h}_1^\dagger \mathbf{p}_2\right) \log \frac{1}{p\left(x_1 | y_1, \mathbf{h}_1^\dagger \mathbf{p}_1, \mathbf{h}_1^\dagger \mathbf{p}_2\right)} dy_1 d(\mathbf{h}_1^\dagger \mathbf{p}_1) d(\mathbf{h}_1^\dagger \mathbf{p}_2) \\ &= \sum_{x_1} \sum_{x_2} \int_{y_1} \int_{\mathbf{h}_1^\dagger \mathbf{p}_1} \int_{\mathbf{h}_1^\dagger \mathbf{p}_2} p\left(x_1, x_2, y_1, \mathbf{h}_1^\dagger \mathbf{p}_1, \mathbf{h}_1^\dagger \mathbf{p}_2\right) \log \frac{\sum_{x_1'} \sum_{x_2'} p\left(y_1 | x_1', x_2', \mathbf{h}_1^\dagger \mathbf{p}_1, \mathbf{h}_1^\dagger \mathbf{p}_2\right)}{\sum_{x_2'} p\left(y_1 | x_1, x_2', \mathbf{h}_1^\dagger \mathbf{p}_1, \mathbf{h}_1^\dagger \mathbf{p}_2\right)} dy_1 d(\mathbf{h}_1^\dagger \mathbf{p}_1) d(\mathbf{h}_1^\dagger \mathbf{p}_2) \end{aligned} \tag{50}$$

where $x_1' \in \chi_1$ and $x_2' \in \chi_2$. Conditioned on the channel and the precoder, there is one source of randomness, i.e. noise. So (50) can be extended as

$$\begin{aligned} \mathcal{H}\left(X_1 | Y_1, \mathbf{h}_1^\dagger, \mathbf{P}\right) &= \frac{1}{M_1 M_2} \sum_{\mathbf{x}} E_{z_1} \log \frac{\sum_{\mathbf{x}'} \exp\left[-\frac{1}{N_0}\left|\mathbf{h}_1^\dagger \mathbf{p}_1 x_1 + \mathbf{h}_1^\dagger \mathbf{p}_2 x_2 + z_1 - \mathbf{h}_1^\dagger \mathbf{p}_1 x_1' - \mathbf{h}_1^\dagger \mathbf{p}_2 x_2'\right|^2\right]}{\sum_{x_2'} \exp\left[-\frac{1}{N_0}\left|\mathbf{h}_1^\dagger \mathbf{p}_2 x_2 + z_1 - \mathbf{h}_1^\dagger \mathbf{p}_2 x_2'\right|^2\right]} \\ &= \frac{1}{M_1 M_2} \sum_{\mathbf{x}} E_{z_1} \log \frac{\sum_{\mathbf{x}'} \exp\left[-\frac{1}{N_0}\left|\mathbf{h}_1^\dagger \mathbf{P}\left(\mathbf{x} - \mathbf{x}'\right) + z_1\right|^2\right]}{\sum_{x_2'} \exp\left[-\frac{1}{N_0}\left|\mathbf{h}_1^\dagger \mathbf{P}\left(\mathbf{x} - \mathbf{x}_2'\right) + z_1\right|^2\right]} \end{aligned} \tag{51}$$

where $M_2 = |\chi_2|$, $\mathbf{x} = [x_1\ x_2]^T$, $\mathbf{x}' = \left[x_1'\ x_2'\right]^T$ and $\mathbf{x}_2' = \left[x_1\ x_2'\right]^T$. The mutual information for UE-1 can be rewritten as

$$I\left(Y_1; X_1 | \mathbf{h}_1^\dagger, \mathbf{P}\right) = \log M_1 - \frac{1}{M_1 M_2} \sum_{\mathbf{x}} E_{z_1} \log \frac{\sum_{\mathbf{x}'} p\left(y_1 | \mathbf{x}', \mathbf{h}_1^\dagger, \mathbf{P}\right)}{\sum_{x_2'} p\left(y_1 | \mathbf{x}_2', \mathbf{h}_1^\dagger, \mathbf{P}\right)} \tag{52}$$

The above quantities can be easily approximated using sampling (Monte-Carlo) methods with N_z realizations of noise and N_{h_1} realizations of the channel $\mathbf{h}_1^\dagger$ where the precoding matrix depends on the channel. So we can rewrite (52) as (53)

$$I\left(Y;X_1|\mathbf{h}_1^\dagger\mathbf{p}_1,\mathbf{h}_1^\dagger\mathbf{p}_2\right)=\log M_1-\frac{1}{M_1M_2N_zN_{h_1}}\sum_{x_1}\sum_{x_2}\sum_{\mathbf{h}_1}^{N_{h_1}}\sum_{z_1}^{N_z}\log\frac{\sum_{x_1'}\sum_{x_2'}\exp\left[-\frac{1}{N_0}\left|y_1-\mathbf{h}_1^\dagger\mathbf{p}_1x_1'-\mathbf{h}_1^\dagger\mathbf{p}_2x_2'\right|^2\right]}{\sum_{x_2'}\exp\left[-\frac{1}{N_0}\left|y_1-\mathbf{h}_1^\dagger\mathbf{p}_1x_1-\mathbf{h}_1^\dagger\mathbf{p}_2x_2'\right|^2\right]}$$

$$=\log M_1-\frac{1}{M_1M_2N_zN_{h_1}}\sum_{x_1}\sum_{x_2}\sum_{\mathbf{h}_1}^{N_{h_1}}\sum_{z_1}^{N_z}\log\frac{\sum_{x_1'}\sum_{x_2'}\exp\left[-\frac{1}{N_0}\left|\mathbf{h}_1^\dagger\mathbf{p}_1x_1+\mathbf{h}_1^\dagger\mathbf{p}_2x_2+z_1-\mathbf{h}_1^\dagger\mathbf{p}_1x_1'-\mathbf{h}_1^\dagger\mathbf{p}_2x_2'\right|^2\right]}{\sum_{x_2'}\exp\left[-\frac{1}{N_0}\left|\mathbf{h}_1^\dagger\mathbf{p}_2x_2+z_1-\mathbf{h}_1^\dagger\mathbf{p}_2x_2'\right|^2\right]} \tag{53}$$

Similarly the mutual information for UE-2 is given as

$$I\left(Y_2;X_2|\mathbf{h}_2^\dagger,\mathbf{P}\right)=\log M_2-\frac{1}{M_1M_2}\sum_{\mathbf{x}}E_{z_2}\log\frac{\sum_{\mathbf{x}'}p\left(y_2|\mathbf{x}',\mathbf{h}_2^\dagger,\mathbf{P}\right)}{\sum_{x_1'}p\left(y_2|\mathbf{x}_1',\mathbf{h}_2^\dagger,\mathbf{P}\right)} \tag{54}$$

where $\mathbf{x}_1^{'}=\left[x_1^{'}\ x_2\right]^T$.

For the case of single-user MIMO mode, the mutual information is given by

$$I\left(Y_1;X_1|\mathbf{h}_1^\dagger,\mathbf{p}_1\right)=\log M_1-\mathcal{H}\left(X_1|Y_1,\mathbf{h}_1^\dagger,\mathbf{p}_1\right) \tag{55}$$

where the second term is given by

$$\begin{aligned}\mathcal{H}\left(X_1|Y_1,\mathbf{h}_1^\dagger,\mathbf{p}_1\right)&=\sum_{x_1}\int_{y_1}\int_{\mathbf{h}_1^\dagger\mathbf{p}_1}p\left(x_1,y_1,\mathbf{h}_1^\dagger\mathbf{p}_1\right)\log\frac{1}{p\left(x_1|y_1,\mathbf{h}_1^\dagger\mathbf{p}_1\right)}dy_1d(\mathbf{h}_1^\dagger\mathbf{p}_1)\\&=\sum_{x_1}\int_{y_1}\int_{\mathbf{h}_1^\dagger\mathbf{p}_1}p\left(x_1,y_1,\mathbf{h}_1^\dagger\mathbf{p}_1\right)\log\frac{\sum_{x_1'}p\left(y_1|x_1',\mathbf{h}_1^\dagger\mathbf{p}_1\right)}{p\left(y_1|x_1,\mathbf{h}_1^\dagger\mathbf{p}_1\right)}dy_1d(\mathbf{h}_1^\dagger\mathbf{p}_1)\\&=\frac{1}{M_1N_zN_{h_1}}\sum_{x_1}\sum_{\mathbf{h}_1^\dagger}^{N_{h_1}}\sum_{z_1}^{N_z}\log\frac{\sum_{x_1'}\exp\left[-\frac{1}{N_0}\left|y_1-\mathbf{h}_1^\dagger\mathbf{p}_1x_1'\right|^2\right]}{\exp\left[-\frac{1}{N_0}\left|y_1-\mathbf{h}_1^\dagger\mathbf{p}_1x_1\right|^2\right]}\end{aligned} \tag{56}$$

where N_{h_1} are the number of channel realizations of the channel $\mathbf{h}_1^\dagger$. Note that the precoding vector $\mathbf{p}_1$ is dependent on the channel $\mathbf{h}_1^\dagger$.

Author details

Rizwan Ghaffar[1,⋆], Raymond Knopp[2] and Florian Kaltenberger[2]

⋆ Address all correspondence to: rizwan.ghaffar@eurecom.fr

1 Samsung Research America, USA
2 EURECOM, France

http://dx.doi.org/10.5772/57134

References

[1] Alamouti, S. [1998]. A simple transmit diversity technique for wireless communications, *IEEE Journal on Selected Areas in Communications* 16(8): 1451–1458.

[2] Au-Yeung, C. K. & Love, D. J. [2007]. On the performance of random vector quantization limited feedback beamforming in a MISO system, *IEEE Transactions on Wireless Communications* 6(2): 458 –462.

[3] Brunel, L. [2004]. Multiuser detection techniques using maximum likelihood sphere decoding in multicarrier CDMA systems, *IEEE Transactions on Wireless Communications* 3(3): 949 – 957.

[4] Caire, G., Taricco, G. & Biglieri, E. [1998]. Bit-interleaved Coded Modulation, *IEEE Transactions on Information Theory* 44(3): 927–946.

[5] Choi, J. W., Singer, A., Lee, J. & Cho, N. I. [2010]. Improved linear soft-input soft-output detection via soft feedback successive interference cancellation, *IEEE Transactions on Communications* 58(3): 986 –996.

[6] Gesbert, D., Kountouris, M., Heath, R., Chae, C.-B. & Salzer, T. [2007]. Shifting the MIMO paradigm, *IEEE Signal Processing Magazine* 24(5): 36 –46.

[7] Ghaffar, R. & Knopp, R. [2010]. Making Multiuser MIMO work for LTE, *IEEE 21-st International Symposium on Personal, Indoor and Mobile Radio Communications (PIMRC 2010)*, Istanbul.

[8] Ghaffar, R. & Knopp, R. [2011]. Interference-Aware Receiver Structure for Multi-User MIMO and LTE, *EURASIP Journal on Wireless Communications and Networking* .

[9] Ghaffar, R. & Knopp, R. [2012]. Interference Suppression Strategy for Cell-Edge Users in the Downlink, *IEEE Transactions on Wireless Communications* 11(1): 154 –165.

[10] Gradshteyn, I. & Ryzhik, I. [2000]. *Table of Integrals, Series, and Products*, Academic Press, San Diego, USA.

[11] Jindal, N. [2006]. MIMO broadcast channels with finite rate feedback, *IEEE Transactions on Information Theory* 52: 5045âĂŞ–5060.

[12] Lamare, R. d. & Sampaio-Neto, R. [2008]. Minimum Mean-Squared Error Iterative Successive Parallel Arbitrated Decision Feedback Detectors for DS-CDMA Systems, *IEEE Transactions on Communications* 56(5): 778 –789.

[13] Li, X., Chindapol, A. & Ritcey, J. [2002]. Bit-interleaved coded modulation with iterative decoding and 8 PSK signaling, *IEEE Transactions on Communications* 50(8): 1250 – 1257.

[14] Love, D. & Heath Jr., R. [2003]. Equal gain transmission in multiple-input multiple-output wireless systems, *IEEE Transactions on Communications* 51(7): 1102 – 1110.

[15] Love, D., Heath, R., Lau, V., Gesbert, D., Rao, B. & Andrews, M. [2008]. An overview of limited feedback in wireless communication systems, *IEEE Journal on Selected Areas in Communications* 26(8): 1341 –1365.

[16] LTE [2009a]. *Evolved Universal Terrestrial Radio Access (E-UTRA); Channel Coding and Multiplexing, Release 8, V.8.6.0*, 3GPP TS 36.212.

[17] LTE [2009b]. *Evolved Universal Terrestrial Radio Access (E-UTRA); Physical Layer Procedures, Release 10, V.8.6.0*, 3GPP TS 36.213.

[18] LTE [June 2011]. *Evolved Universal Terrestrial Radio Access (E-UTRA); User Equipment (UE) radio transmission and reception*, 3GPP TS 36.101 Version 10.3.0 Release 10.

[19] LTE-A [2011]. *Evolved Universal Terrestrial Radio Access (E-UTRA); Physical Layer Procedures, Release 10, V.10.1.0*, 3GPP TS 36.213.

[20] Lupas, R. & Verdu, S. [1989]. Linear multiuser detectors for synchronous code-division multiple-access channels, *IEEE Transactions on Information Theory* 35(1): 123 –136.

[21] Qi, X., Alouini, M.-S. & Ko, Y.-C. [2003]. Closed-form analysis of dual-diversity equal-gain combining over Rayleigh fading channels, *IEEE Transactions on Wireless Communication* 2(6): 1120 – 1125.

[22] Sesia, S., Toufik, I. & Baker, M. [2009]. *LTE, The UMTS Long Term Evolution: From Theory to Practice*, Wiley.

[23] Speth, M., Jansen, A. & Meyr, H. [2000]. Iterative multiuser detection for bit interleaved coded modulation, *IEEE International Conference on Communications, ICC 2000*, Vol. 2, pp. 894 –898 vol.2.

[24] Telatar, I. E. [1999]. Capacity of multiâĂŞantenna Gaussian channels, *European Transactions on Telecommunications* 10(6): 585–595.

[25] Verdu, S. [1998]. *Multiuser Detection*, Cambridge University Press, U.K.

[26] Wang, X. & Poor, H. [1999]. Iterative (turbo) soft interference cancellation and decoding for coded CDMA, *IEEE Transactions on Communications* 47(7): 1046 –1061.

[27] Zakhour, R., Ho, Z. K. M. & Gesbert, D. [2009]. Distributed beamforming coordination in multicellular MIMO systems, *IEEE 69th Vehicular Technology Conference,VTC-Spring. April, 26-29, 2009, Barcelona, Spain*.

[28] Zarikoff, B., Cavers, J. & Bavarian, S. [2007]. An iterative groupwise multiuser detector for overloaded MIMO applications, *IEEE Transactions on Wireless Communications* 6(2): 443 –447.

[29] Zhang, Q. [1997]. Probability of error for equal-gain combiners over Rayleigh channels: some closed-form solutions, *IEEE Transactions on Communications* 45(3): 270 –273.